INTERNATIONAL JOURNAL OF CLIMATOLOGY
Int. J. Climatol. (in press)
Published online in Wiley InterScience
(www.interscience.wiley.com) DOI: 10.1002/joc.1525

RMetS
ROYAL METEOROLOGICAL SOCIETY

ENSO history recorded in *Agathis australis* (kauri) tree rings. Part A: kauri's potential as an ENSO proxy

A. M. Fowler,[a]* G. Boswijk,[a] J. Gergis[b] and A. Lorrey[a,c]

[a] *School of Geography, Geology, and Environmental Science, The University of Auckland, Private Bag 92019, Auckland, New Zealand*
[b] *Biological, Earth and Environmental Sciences, The University of New South Wales, Sydney NSW 2052 Australia*
[c] *National Institute of Water and Atmospheric Research, Auckland, New Zealand*

ABSTRACT: Although many of the main characteristics of the El Niño-Southern Oscillation (ENSO) phenomenon have been established, uncertainties remain concerning its multidecadal- to millennial-scale evolution. Because of the shortness of the instrumental record, we need to resort to proxy-based reconstructions to investigate ENSO's history prior to the mid 19th century, but the available proxy data is limited in both time and space. Here we investigate the potential for ENSO reconstruction from the tree rings of *Agathis australis* (kauri). Kauri is a long-lived endemic New Zealand conifer and grows in an ENSO teleconnection region not previously represented in ENSO multi-proxy studies. A high quality 423 year kauri regional master chronology (AD 1580–2002) is constructed. Statistical analysis of the period AD 1876–2002 confirms previous findings that kauri tree rings carry a strong regional-scale climate signal and that ENSO is a significant contributor (predominantly via the western pole of the Southern Oscillation). Kauri carries a signal of both ENSO phases, but with a slight El Niño bias. Growth sensitivity is primarily registered through a five-season window, extending from March (prior to growth initiation in September) through to the following May, with strongest relationships across the middle three seasons (June–February). Relationships appear to be stationary. We conclude that kauri has sufficient ENSO event capture skill to make it a useful addition to future multi-proxy ENSO reconstruction efforts. It may also have potential for stand-alone reconstruction of multidecadal- to millennial-scale evolution of ENSO activity, especially ENSO robustness.

KEY WORDS El Niño-Southern Oscillation; ENSO; tree rings; kauri; *Agathis australis*; New Zealand; palaeoclimatology; dendroclimatology

Received 28 March 2006; Revised 14 February 2007; Accepted 15 February 2007

1. Introduction

The El Niño-Southern Oscillation (ENSO) phenomenon is a vast atmosphere-ocean interaction centred on the tropical Pacific Ocean, and is one of the most important sources of global-scale natural climate variability (Diaz and Markgraf, 1992, 2000; Allan *et al*., 1996). Research over several decades has defined ENSO's main characteristics and identified teleconnections with the climate of many extra-tropical regions (e.g. Allan, 1988; Mann *et al*., 2000; Reason *et al*., 2000). However, no complete theory is yet capable of explaining all aspects of ENSO. Key uncertainties include: (1) whether ENSO is a late Holocene phenomenon only; (2) the stability in time of observed 20th century teleconnections, and; (3) how the character of ENSO has varied on decadal to millennial time scales. A specific question arising in the context of the last point is whether unusual ENSO activity since the late 20th century (more frequent and intense El Niños and a protracted El Niño in the early 1990s) represents a fundamental change in state, or a return to conditions previously experienced.

Available instrumental records are not long enough to resolve century-scale ENSO variability, nor to ascertain if observed decadal-scale variability is typical (Allan and D'Arrigo, 1999). Addressing such questions requires high resolution (annual or better) proxy records of climate, from sources such as tree rings, ice cores, and coral, and from historical records of related phenomena (e.g. droughts). However, with the notable exception of coral, most ENSO-sensitive proxy data come from teleconnection regions, rather than from the tropical Pacific core region. Because teleconnection patterns are known to vary in time (Mann *et al*., 2000), it is recognized that a comprehensive spatial network of ENSO-sensitive proxies is desirable to capture large-scale ENSO variability (Stahle *et al*., 1998).

In the context of an ideal network for ENSO reconstruction (ENSO-sensitive proxies from all significant teleconnection regions), the current situation is deficient (Figure 1). Some significant teleconnection regions (e.g. southern Africa) are unrepresented, the Southern Hemisphere is poorly represented (especially outside the tropics), and there is unequal weighting of the eastern and

* Correspondence to: A. M. Fowler, School of Geography, Geology, and Environmental Science, The University of Auckland, Private Bag 92019, Auckland, New Zealand. E-mail: a.fowler@auckland.ac.nz

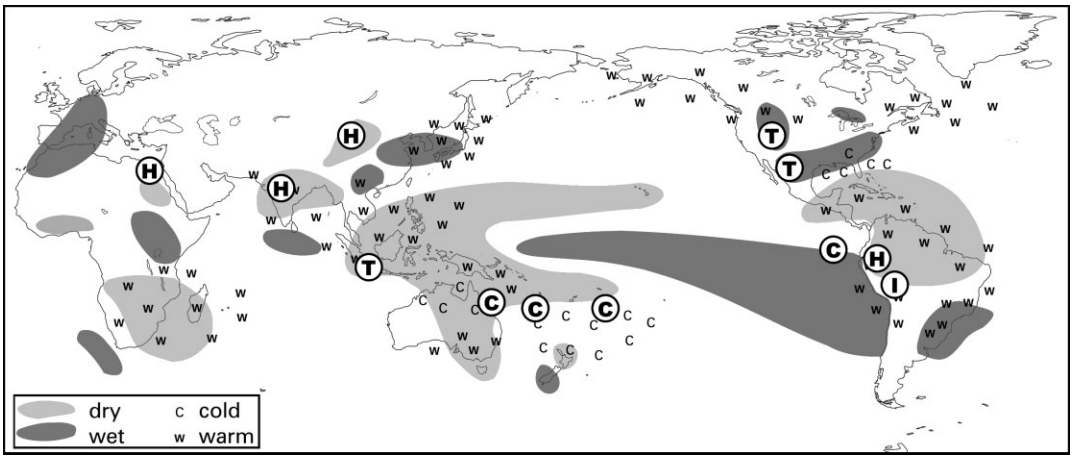

Figure 1. Global teleconnection patterns associated with El Niño events (modified after Allan *et al*., 1996), with superimposed ENSO-sensitive, multi-century, high resolution proxies identified by Gergis *et al*. (2004). 'C' denotes coral proxies from the Great Barrier Reef (Hendy *et al*., 2002, 2003), New Caledonia (Quinn *et al*., 1998), Rarotonga (Linsley *et al*., 2000), and Galapagos (Dunbar *et al*., 1994). 'T' denotes tree-ring proxies from Indonesia (Berlage, 1931; D'Arrigo *et al*., 1994), the southwest USA (Stahle *et al*., 1998; D'Arrigo *et al*., 2005), and Mexico (Stahle *et al*., 1998; Cleaveland *et al*., 2003; D'Arrigo *et al*., 2005). 'I' denotes ice core proxy from Quelccaya ice cap, Peru (Thompson *et al*., 1984; Thompson *et al*., 2000). 'H' denotes historical drought, precipitation, and runoff records from South America (Quinn and Neal, 1992; Ortlieb, 2000), India, Egypt, and China (Whetton and Rutherfurd, 1994).

western Pacific ENSO poles. Such deficiencies have the potential to bias ENSO reconstructions, especially further back in time when important, but relatively short, ENSO tropical core region proxies (coral and Indonesian teak tree rings) are unavailable. As a consequence, the early proxy record is dominated by tree rings from the southern North America teleconnection region (e.g. D'Arrigo *et al*., 2005).

New Zealand and Tasmania have potential in terms of improving the proxy database for ENSO reconstruction. Both are known ENSO teleconnection regions (Figure 1) and each has significant areas of old-growth forest, from which multi-century (in some cases multi-millennial) tree-ring chronologies have been derived (Cook *et al*., 2000; Xiong and Palmer, 2000; Cook *et al*., 2002; Boswijk *et al*., 2006). ENSO-sensitive proxies from the southwest Pacific would also be helpful in reducing potential bias in future multi-proxy ENSO reconstructions associated with the present poor representation of the Southern Hemisphere and the western ENSO pole.

Agathis australis (D. Don) Lindley (kauri) is a New Zealand conifer with considerable potential as an ENSO proxy. It is a large endemic canopy emergent, occurring naturally and abundantly north of 38 °S (Figure 2), often in relatively undisturbed environments. Ages in excess of 600 years are common and individual trees older than 1000 years are not unusual. Abundant material is also available from 19th and early 20th century logging, as relic material in museums and timbers in colonial-era buildings. Large quantities of sub-fossil wood are also preserved in swamps, including much late-Holocene material (Boswijk *et al*., 2006).

Kauri growth is enhanced (suppressed) by cool-dry (warm-wet) conditions in the growing season, especially in the austral spring i.e. September October November (SON) (Buckley *et al*., 2000). This relationship to climate is fortuitous in terms of ENSO reconstruction potential, because such conditions are respectively associated with El Niño and La Niña events in the far north of New Zealand (Gordon, 1985; Mullan, 1995). Moreover, the strongest relationships between kauri growth and climate occur during SON, coincident with the peak strength of the teleconnection between ENSO and New Zealand climate (Mullan, 1995). Recognition of these juxtapositions led to identification of kauri's potential as an ENSO proxy by Fowler *et al*. (2000).

Recent research on kauri tree rings has focused on improving the quality of the database and refining understanding of the kauri-ENSO relationship. Notable developments include:

(1) Bridging the gap between subfossil late-Holocene kauri tree-ring chronologies and those derived for living trees, resulting in a 3722 year calendar-dated tree-ring chronology (Boswijk *et al*., 2006). This is the longest, continuous, annually-resolved, ENSO-sensitive proxy record we know of.
(2) Resolution of low sample depth issues during the last two decades of the 20th century by resampling two sites (Gergis *et al*., 2005a,b) and the addition of two new sites (Lorrey, 2005; Boswijk and Ogden, 2005).
(3) Improved understanding of the seasonal growth characteristics of kauri (Fowler *et al*., 2005).
(4) Increased knowledge of atmospheric circulation forcing responsible for the negative correlations between kauri growth and both surface air temperature and precipitation (Fowler, 2005).

This paper is Part A of a two-phase investigation. Here we definitively establish kauri's capabilities (and limitations) as an ENSO proxy. This coincides with the release of the relevant tree-ring data (here and to the International Tree-Ring Data Bank) and is intended

DOI: 10.1002/joc

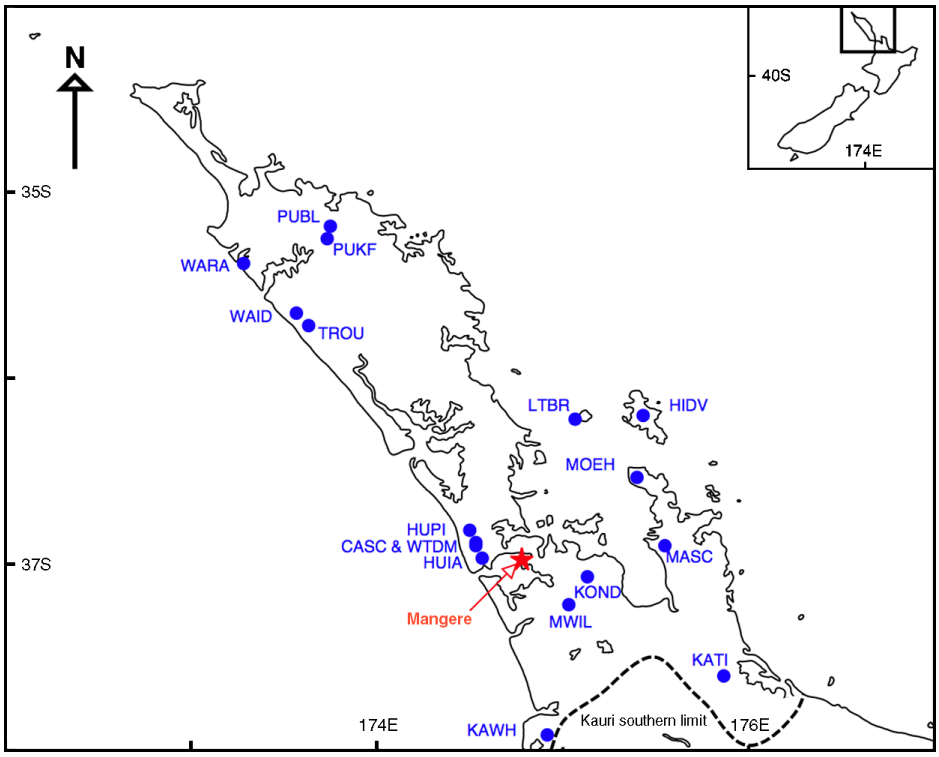

Figure 2. Locations of 17 modern crossdated kauri site chronologies (dots) and the Mangere climate station (star). This figure is available in colour online at www.interscience.wiley.com/ijoc

to facilitate the incorporation of kauri in future multi-proxy ENSO research. The paper also forms the basis for interpretation of multi-century ENSO activity in Part B (Fowler, this issue).

2. Data

2.1. Tree-ring data

Fowler *et al.* (2004) reviewed the modern kauri data base available by mid-2003 (196 trees from 14 sites). By December 2005, 34 more trees had been added from further sampling at two sites (PUKF, TROU) and the addition of two others (HIDV, WTDM) (Table I). Sample depth peaked at 202 trees from all sites in AD 1900 and exceeded 100 trees from at least 13 sites from AD 1750–1981. Sample depth declined in a complex manner prior to AD 1750 and after AD 1981 as trees and whole sites dropped out. Prior to AD 1600 there were fewer than 30 trees from no more than nine sites.

Standardization is routine practice in dendroclimatology, designed to remove non-climatic trend from the tree-ring data, such as the typical decline in ring-widths as trees age, and decadal-scale variation caused by competition in closed-canopy forests (Fritts, 1976). This is commonly done by fitting a flexible curve to a ring-width time series, then dividing observed ring-widths by the corresponding values for that curve. The resulting indices for each radii have a mean of about one and each value represents the fraction of 'expected' growth at that time. Fowler *et al.* (2004) maximized the statistical quality of kauri tree-ring chronologies by standardizing data using 20 year splines (50% frequency response at 20 years). However, because such flexible standardization curves remove multi-decadal trend in the data (of primary interest here), a replicate standardization was undertaken using 200 year splines. Standardization was undertaken with the computer program ARSTAN (Cook, 1985; Holmes, 1986).

Standardized radii from the same tree were averaged to produce tree means. Tree means were then averaged to produce site chronologies and two kauri master chronologies: AGAUm05a (built from series standardized using 20 year splines) and AGAUm05b (200 year splines) (Figure 3, Appendix). The masters were built by averaging tree-ring indices of all trees, except those from the anomalous high altitude Mt Moehau (MOEH, see Section 3). For brevity and clarity the masters are hereafter respectively referred to as 'K20' and 'K200', and the terms 'spline20' and 'spline200' are used to indicate the standardization applied.

On the basis of the statistical analysis of the kauri data set available by mid-2003, Fowler *et al.* (2004) concluded that high quality kauri master chronologies could be built for the period AD 1597–1996. As a consequence of the updated data set (Table I), the analysis period used here was extended to AD 1580–2002 (Figure 3), based on 20+ trees and expressed population signal (EPS) >0.8. [EPS is a statistical measure of the quality of tree-ring chronologies, derived from the cross-correlation matrix of all series comprising the chronology. Values range from zero to one, where one represents a hypothetical perfect

DOI: 10.1002/joc

Table I. Kauri modern tree-ring chronology sites added or revised since Fowler *et al*. (2004).

Code	Location	Trees (cores)	Dates (AD)	Comments and References
HIDV	Hidden Valley, Great Barrier Island (36° 12′S 175° 26′E) Altitude: 220 m Aspect: E	13 (20)	1697–2003	1999: Ten cores taken from five trees. 2004: additional core taken from each tree, and four additional trees and a rotted log cored. Boswijk and Ogden (2005).
PUKF	Puketi forest South (35° 15′S 173° 44′E) Altitude: 290 m Aspect: N	22 (47)	1504–2002	Original chronology (Ahmed M. 1984. *Ecological and Dendrochronological Studies on Agathis australis Salisb. (kauri)*. Unpubl. PhD thesis, The University of Auckland, Auckland). spanned 1780–1982 (19 radii, 10 trees) developed from pooling material from the Loop track and Te Harua in southern Puketi. 2003: 39 cores (15 trees) from 'Loop Track' (Waihoanga Gorge, southern Puketi forest). 27 crossdated radii (12 trees) merged with original data, resulting in a 297-year extension. Ahmed and Ogden (1985), Gergis *et al*. (2005a).
TROU	Trounson Kauri Park (35° 43′S 173° 38′E) Altitude: 175 m Aspect: N	26 (52)	1529–2002	Original chronology (Ahmed M. 1984. *Ecological and Dendrochronological Studies on Agathis australis Salisb. (kauri)*. Unpubl. PhD thesis, The University of Auckland, Auckland). Spanned 1668–1980 (19 radii, 13 trees). 2004: cores remeasured and crossdated, yielding an additional 10 radii (three trees). 2004: 40 cores taken from 15 trees in the NE of the park. 23 crossdated radii (10 trees) merged with original data, resulting in a 161-year extension. Ahmed and Ogden (1985), Gergis *et al*. (2005b).
WTDM	Waitakere Dam (36° 54′S 174° 32′E) Altitude: 210 m Aspect: N-NW	7 (22)	1728–2002	Kauri originally located on well-drained ridge, but now near lake-level following construction of Waitakere Dam (1907 and 1927). Sampled February, 2004. Lorrey (2005).

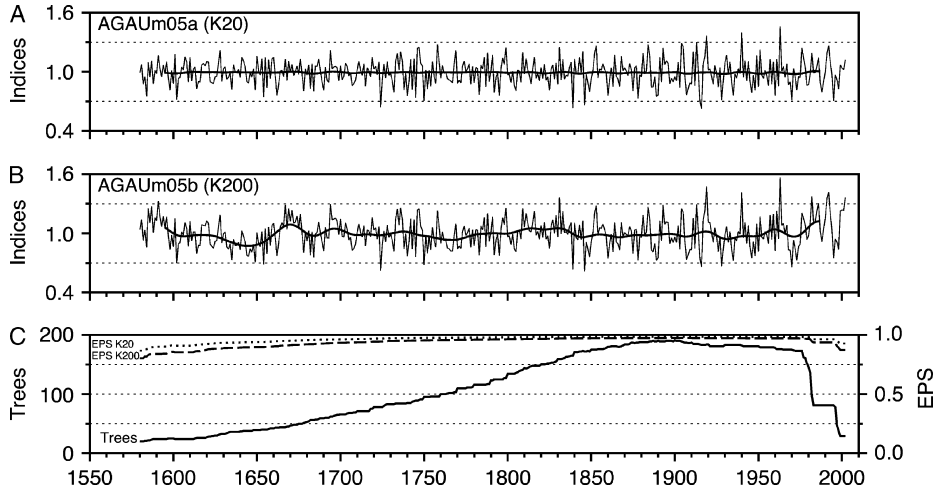

Figure 3. Kauri master chronologies AGAUm05a (K20) and AGAUm05b (K200), sample depth (Trees), and evolving expressed population signal (EPS). Heavy lines in A and B show smoothed series, derived using a 31-year Hanning window (Lyons, 1997).

chronology. Wigley *et al*. (1984) derived EPS from mathematical first principles for chronologies computed from one series per tree. This was extended to a more general form of variable cores per tree by Briffa and Jones (1990). The latter is used here.] For AD 1580–1996, the 20+ trees are from at least eight sites. The number of sites declines after 1996, to a low of four from 1999 (HIDV, PUKF, TROU, WTDM). Note that the update work at PUKF and TROU also resolved a spatial representation problem of no post-1981 data from any of the five northern sites shown in Figure 2.

2.2. Climate data

Climate data used are monthly precipitation and surface air temperature data for Auckland, near the centre of kauri's growth range. The data are homogenized records (1853–2001) for the Auckland reference site at Mangere (Figure 2), provided by Jim Salinger (pers. com.). We

DOI: 10.1002/joc

also used monthly modelled 20th century soil water content for a kauri forest near Auckland (Fowler and Adams, 2004).

Several monthly indices of ENSO (1876–2003) were used. The oceanic component was represented by sea surface temperature (SST) in the Niño 3.4 zone (5°N–5°S, 120°–170°W). Post-1949 SST anomalies were obtained from the National Oceanic and Atmospheric Association (NOAA) Climate Prediction Center. Pre-1950, we used the Trenberth and Stepaniak (2001) reconstruction, derived from the Hadley Centre Sea Ice and SST data set. The atmospheric component was represented by mean sea level pressure (MSLP) data for Tahiti and Darwin and by the well-known Southern Oscillation Index (SOI), derived from these. These data were obtained from the Australian Bureau of Meteorology. We also used the coupled ENSO index (CEI) of Gergis and Fowler (2005), a composite index derived from the Niño 3.4 SSTs and the SOI.

MSLP compositing analysis used the Hadley Centre 5° latitude by 5° longitude, global gridded monthly MSLP data set (1871–1994, version GMSLP2.1f), evaluated by Basnett and Parker (1997).

3. Evidence of an ENSO Signal in Kauri Tree Rings

This section presents evidence that kauri tree rings carry a significant ENSO signal. Tree-ring correlation analyses (Section 3.1) demonstrate strong regional-scale climate forcing of kauri growth, and show that the signal associated with that forcing is amplified in master chronologies built from pooled data (updating Fowler *et al*. (2004)). Response function analyses (Section 3.2) reinforce the argument of pervasive regional-scale forcing and provide evidence that ENSO is a significant component (developing and revising Fowler *et al*. (2000)). MSLP composite mapping (Section 3.3) provides additional evidence of ENSO forcing, and a partial physical mechanism explaining correlations of kauri with the SOI (based on Fowler, 2005).

3.1. Tree-ring correlation analyses

Fowler *et al*. (2004) analysed inter-site correlations of 13 high quality kauri tree-ring chronologies over an optimal quality time period (1840–1920). They identified no anomalous sites and only weak evidence of spatial groupings. From this, and other analyses, they concluded that building kauri master chronologies by pooling data from across kauri's growth range is justified. Our updates to TROU and PUKF (Table I) improved the correlation statistics for the two sites but did not materially change the results from which Fowler *et al*. (2004) drew their conclusions.

The purpose of building the kauri masters was to maximize any common signal across kauri's growth range. We tested this by comparing mean inter-site correlations with correlations of sites against K20 and K200 (1840–1920). The results show the expected sensitivity of the correlations to the statistical quality (EPS) of site chronologies (Figure 4(A)), which in turn is largely determined by sample depth (Figure 4(B)). More importantly, the results also show much stronger correlations between site chronologies and the kauri masters than with other sites. Additional analyses (not shown) indicated that about one third of the correlation increase (above mean inter-site correlations) is due to the joint presence of trees in the site and master chronologies. Correcting for this gives a net relative increase in explained variance of about 80%. We interpret this as strong evidence that regional-scale forcing is a major determinant of kauri growth. This is consistent with the conclusions reached by Fowler *et al*. (2004), based on principal components analysis.

3.2. Response function analysis

Correlation analysis was used to investigate concurrent and lagged relationships between tree-ring chronologies and selected climate variables. Specifically, seasonal precipitation and mean surface air temperature correlation response functions (Blasing *et al*., 1984; Figure 5)) were constructed for 16 of the 17 kauri tree-ring site

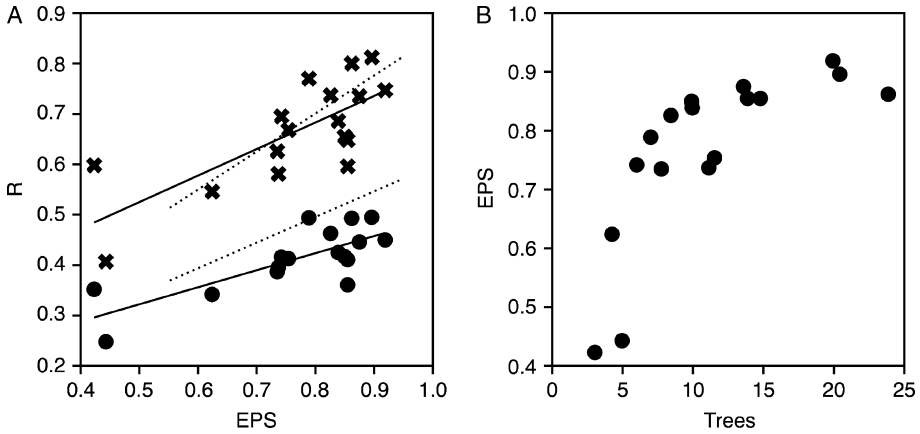

Figure 4. Comparison of mean inter-site and site-master correlations (R), and their dependence on site chronology expressed population signal (EPS), for 1840–1920 (Panel A). EPS is significantly influenced by sample size (Panel B). Mean inter-site correlations (dots in Panel A) are for spline200 site chronologies. Crosses are correlations between these site chronologies and K200. Solid lines are associated linear regression lines. Dashed lines are the equivalent regression lines for spline20 analyses (not shown).

DOI: 10.1002/joc

chronologies, for the period 1853–1996 (WAID excluded because of no data post-1903). Climate data were for the long-term homogenized Auckland climate record. Results for spline200 chronologies show similar correlation patterns across 15 sites (Figure 5, box-and-whiskers plots). MOEH (thin lines) is the only noticeable exception, with a generally weaker and sometimes opposite response, especially for temperature during the growing season and the two prior years. For MOEH, the temperature relationship is positive or near zero over this period, whereas other sites change to a consistently negative relationship from the autumn prior to growth (MAM-1). These results were the basis for excluding MOEH trees from the two kauri master chronologies.

Heavy solid lines in Figure 5 show correlation results for K200. Comparison with the site chronology results shows that the relationship between K200 and climate is generally stronger (higher absolute correlations) than relationships for individual sites. Most seasons have one or more sites with a stronger correlation than K200, but this is rarely sustained over multiple seasons. Two exceptions are CASC (higher correlations with precipitation at lags of 3–4 years) and KATI (stronger negative correlations with temperature from MAM-1 – JJA). These results are encouraging in terms of the validity and usefulness of building the kauri master chronologies. The fact that doing so does not result in an intermediate strength signal, let alone different signals canceling each other, confirms that combining data across sites enhances the climate signal.

Correlation results for precipitation and temperature have similar temporal patterns. Both show weak, but persistent, positive correlations at lags of 2–4 years (MAM-4 – JJA-2), and weak, persistent, negative correlations from the prior autumn (MAM-1), through the growing season, and into the following year. (Tree growth cannot be affected by future climate, so the latter presumably reflects climate persistence.) Results differ between these two common periods. Correlation with seasonal precipitation peaks in the prior spring (SON-1), with a relatively abrupt change to negative correlations by two seasons later, whereas the temperature results show a more gradual transition. Results for modelled soil water (not shown) are qualitatively similar to those for precipitation, except

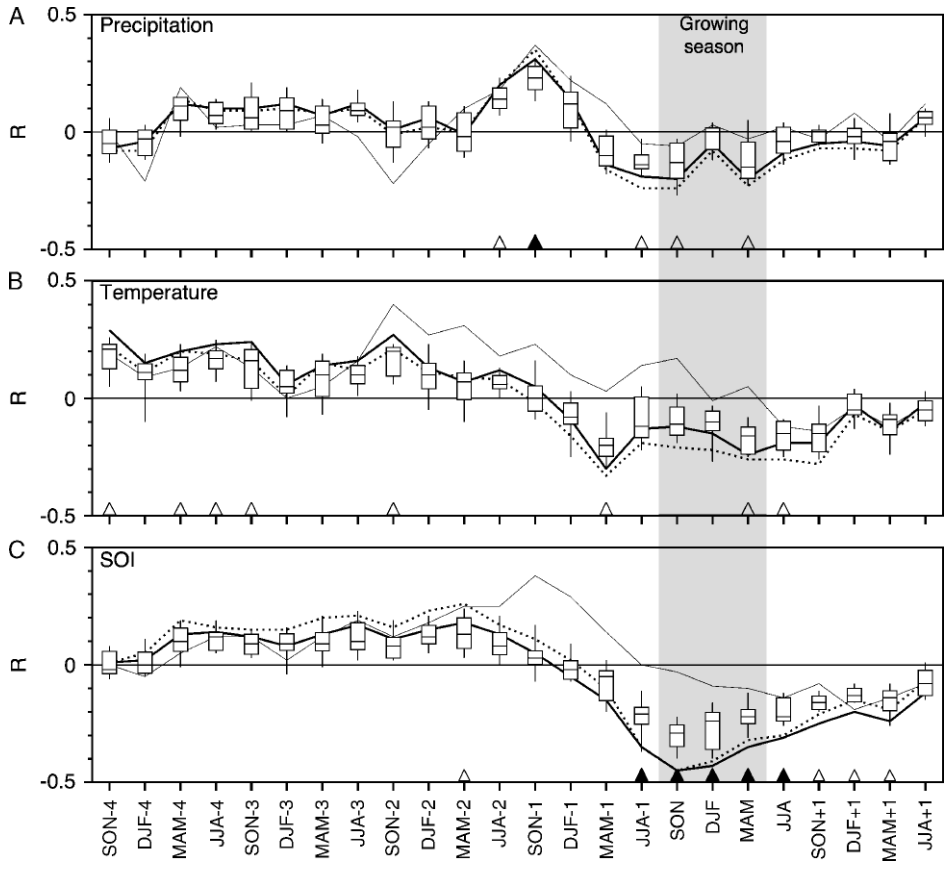

Figure 5. Seasonal correlation response functions. Box-and-whiskers plots (10th, 25th, 50th, 75th, and 90th percentiles) show the correlation (R) distribution of 15 site chronologies (MOEH and WAID excluded) with Auckland precipitation (Panel A) and surface air temperature (Panel B), and with the SOI (Panel C). Lines show R for MOEH (thin), K20 (dotted) and K200 (thick). R for precipitation and temperature is calculated over 1853–1976 (KOND), 1853–1979 (WARA), 1853–1980 (MOEH), 1853–1981 (HUIA, LTBR, MTWL), 1853–1982 (CASC, PUBL), or 1853–1996 (HIDV, HUPI, KATI, KAWH, MASC, PUKF, TROU, WTDM). Calculations of R with the SOI started in 1876 and terminated as above. Season labels without trailing numbers (e.g. 'SON') denote R with climate variables concurrent with the tree growth year (SON, DJF, MAM, JJA). Negative trailing numbers indicate R for seasons up to 4 years previously. Positive numbers denote R with the climate of subsequent seasons. Triangles plotted along the x-axis denote significant relationships, adjusted for serieal autocorrelation (Quenouille, 1952), at the $p < 0.05$ (open) and $p < 0.001$ (solid) levels.

DOI: 10.1002/joc

that the peak lag relationship is delayed to the prior summer (DJF-1) and relationships are stronger (and strongest) over the growing season.

The correlation response function results are consistent with the conclusions of Buckley *et al*. (2000) that kauri growth tends to be enhanced (suppressed) by cool-dry (warm-wet) conditions during the growing season and for the prior autumn and winter, with inverse lag climate-growth relationships for several years prior to the growing season. The biological mechanisms underpinning these repeatedly demonstrated, but somewhat counter-intuitive, results remain uncertain (Fowler *et al*., 2000).

Fowler *et al*. (2000) identified kauri's potential as an ENSO proxy, based on similar response function results to Figure 3(A) and (b), and known ENSO teleconnections to regional climate; namely cool-dry (warm-wet) conditions during El Niño (La Niña) events, peaking in SON (Mullan, 1995). Their most convincing evidence was stronger correlations between the first kauri tree-ring master chronology and the SOI than with either precipitation or temperature. Repeating and expanding their analysis, using the updated tree-ring data set, gave comparable results in terms of pattern (Figure 5(C)). Specifically, there are positive lag correlations for 10 seasons (MAM-4 – JJA-2), three transitional seasons (SON-1 – MAM-1), and negative correlations from the winter prior to growth (JJA-1), through the growing season (SON – MAM). The latter peak in SON and DJF, then gradually decline in strength through MAM and for the following year.

Comparing SOI response function results with those for precipitation and temperature reveals four points of interest. First, MOEH is again clearly anomalous, supporting the decision to exclude MOEH data from the master chronology builds. Second, weak R with the SOI at SON-1 and DJF-1 suggests that the corresponding relatively strong relationships for precipitation and soil water are probably not ENSO-related. Third, the K20/K200 correlations are stronger than most site correlations, especially for the five seasons centred on the growing season (JJA-1 – JJA). This is further evidence of amplification of the common signal in the master chronologies, and is consistent with ENSO being an important contributor to regional forcing. Fourth, the K20/K200 correlations with SOI over the growing season are substantially higher than the precipitation and temperature correlations (2–3+ times explained variance), indicating that ENSO may be the dominant source of regional-scale climate forcing affecting kauri growth.

The K20/K200 response functions (Figure 5) are similar, reflecting nearly identical inter-annual variance (Figure 3). Differences are mostly a consequence of decadal to multi-decadal trend in K200 (e.g. the late 20th century trend to wider rings), coinciding with similar or opposite trends in the climate time series. The effect is clearly evident for temperature (Figure 5(B)), where the K200 correlations are consistently more positive than those for K20. This is caused by positive trends in both temperature and K200, resulting in stronger positive lag correlations and weaker negative correlations, especially during SON and DJF. Negative trend in the SOI (more late 20th century El Niños) has the opposite effect of weakening positive correlations and strengthening negative correlations (Figure 5(C)). Negligible differences between K20 and K200 correlations for the five seasons straddling the growing season (JJA-1 – JJA) suggest that the effect of opposing trends is of similar magnitude to the loss of high frequency signal associated with use of more conservative standardization in the case of K200.

3.3. MSLP composite mapping

We deduce from the negative correlations of the kauri master chronologies with the SOI (Figure 5(C)) that wide (narrow) kauri tree rings are likely to be associated with El Niños (La Niñas). ENSO events are associated with vast spatial patterns of MSLP anomalies (Wallace *et al*., 1998; Trenberth and Caron, 2000), which drive the ENSO teleconnection to New Zealand through changes in prevailing winds, interacting with New Zealand's complex topography (Mullan, 1996). El Niños tend to increase the frequency of cold southwesterlies (associated with a higher incidence of 'zonal regimes' Kidson, 2000), bringing dry conditions to the kauri growth region (Mullan, 1996). La Niñas are associated with a higher incidence of slow-moving or blocking anticyclones southeast of New Zealand, and with increased cyclonic activity in the Tasman Sea. Such conditions result in more frequent warm northerly/northeasterly winds, bringing wetter conditions to the kauri growth region (Mullan, 1996). This is consistent with the negative correlations of kauri tree rings with growing season temperature and precipitation (Figure 5(A) and (B)).

Fowler (2005) further investigated the process links between ENSO and kauri growth by comparing MSLP composite maps for wide and narrow tree rings with equivalent El Niño and La Niña event composites (e.g. Figure 6). For example, Figure 6(B) shows mean September–February MSLP anomalies associated with the one third widest kauri tree rings. September–February was selected because it is the period of maximum kauri growth (Fowler *et al*., 2005), and of peak correlations to the SOI (Figure 5(C)). Comparison of the SOI and kauri composites shows strong similarities in the spatial structure of anomaly patterns of El Niños (La Niñas) and wide (narrow) tree rings. We argue that this is additional evidence that ENSO is an important forcing factor. Nuances, such as differences in strength of relationships for wide and narrow tree rings, and apparent differences in the relative importance of the east and west ENSO poles, are discussed in Section 4.

4. Utility of Kauri as an ENSO Proxy

The previous section makes the case that kauri tree rings carry a significant ENSO signal. Here we explore that relationship in detail, with a view to establishing kauri's utility for ENSO reconstruction. We begin by

DOI: 10.1002/joc

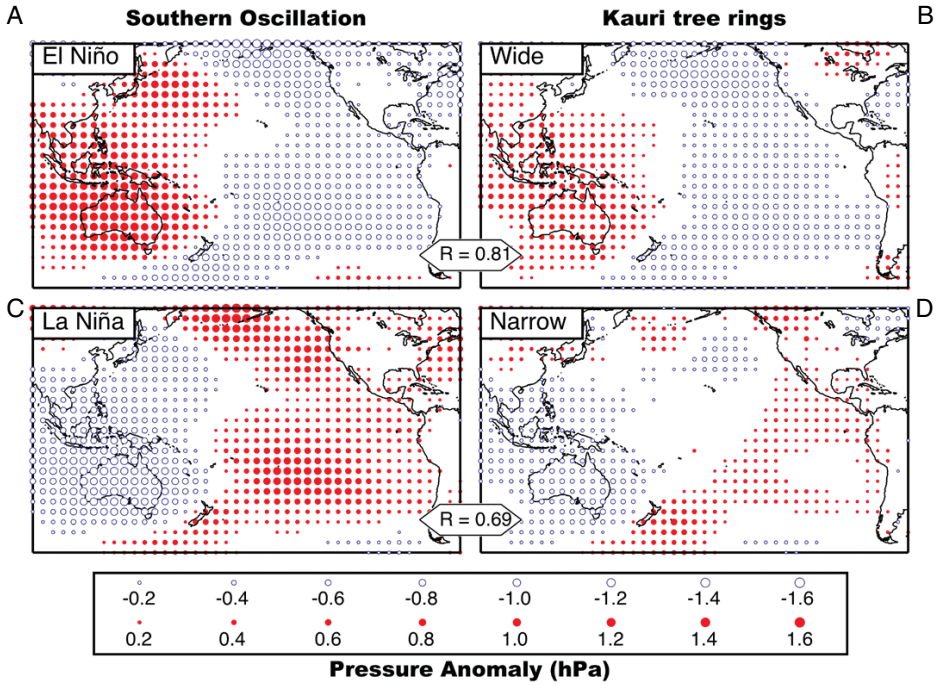

Figure 6. September–February MSLP anomaly composite maps (1901–1994) for the SOI and for kauri tree rings (K20). Each composite map shows mean pressure anomalies associated with the upper or lower third of the SOI and K20 data. See Fowler (2005) for method details. Source: redrawn from Figure 2 in Fowler (2005). This figure is available in colour online at www.interscience.wiley.com/ijoc

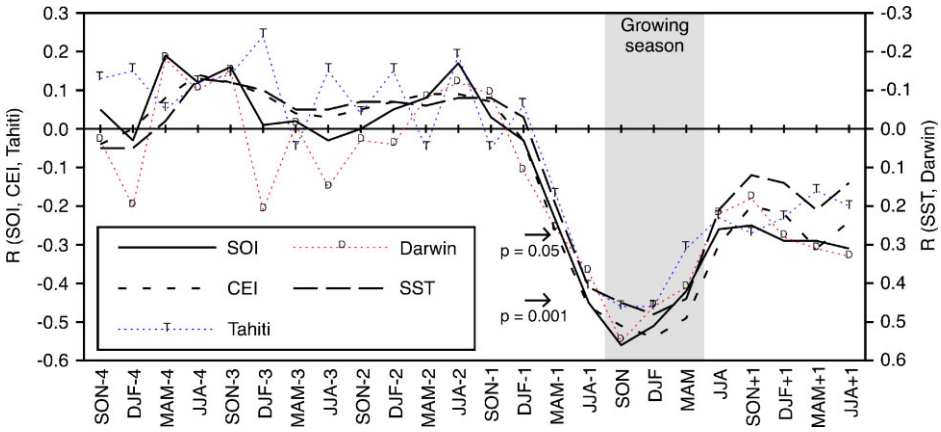

Figure 7. Seasonal correlation response functions – K200 with three ENSO indices (SOI, SST, CEI) and Tahiti and Darwin MSLP. Correlations calculated over 1950–2002. Arrows denote significant relationships at the specified probability levels (no correction for serial correlation necessary). This figure is available in colour online at www.interscience.wiley.com/ijoc

investigating if kauri is sensitive to the atmospheric and/or oceanic components of ENSO (Section 4.1) and establish the temporal response window (Section 4.2). This is followed by a series of analyses determining the nature, strength, and quality of the ENSO signal in kauri (Sections 4.3–4.7). We conclude with an investigation of the stationarity of relationships (Section 4.8).

4.1. Sensitivity to ENSO components (Southern Oscillation, SSTs)

The New Zealand teleconnection to ENSO is usually couched in terms of Southern Oscillation (SO) impacts on regional circulation (e.g. Mullan, 1995, 1996). It is therefore plausible that kauri's ENSO signal represents SO forcing, with no direct process links to SSTs. This would have implications for kauri's ENSO reconstruction potential. To explore this we extended response function analysis to alternative ENSO indices (Figure 7). The atmospheric and oceanic components were represented by the SOI and Niño3.4 SSTs, and the CEI (Gergis and Fowler, 2005) was used as a composite index. Analysis was limited to 1950–2002, to avoid possible SST and CEI low correlation bias, relative to the SOI, associated with pre-1950 SST reconstruction.

For the five seasons of strongest correlations (JJA-1–JJA) K200 correlations with the SOI are mostly higher than with SSTs. This is consistent with the SO teleconnection process link and suggests that kauri is likely to have greatest utility as an SO proxy. But differences are relatively small, presumably reflecting

DOI: 10.1002/joc

the tight coupling of ENSO's atmospheric and oceanic components, and kauri clearly also has potential as a Niño3.4 SST proxy. Interestingly, correlations with the CEI are stronger than with either of the component indices (except for the SOI in SON). However, hereafter we focus on the SOI since this relates most closely to the assumed causal mechanism.

4.2. Temporal response window

Fowler *et al*. (2005) presented results from a four-year kauri growth study, based on monthly (or better) vernier band measurements of 43 kauri trees. They concluded that kauri grows from September to June, with the bulk of the tree ring formed in the austral spring and early summer. A key finding was that October and November alone accounted for 38–50% of the total annual ring width, coincident with the strongest teleconnection patterns between ENSO and the climate of northern New Zealand (Gordon, 1986; Mullan, 1995).

The timing of kauri's growth season is also fortuitous with respect to the typical life cycle of an ENSO event. ENSO events are phase-locked to the annual cycle, preferentially changing sign about March through May (Trenberth and Caron, 2001). Once a change begins, ocean-atmosphere feedbacks result in a typical 12–18 month life cycle (Dunbar, 2000; Diaz *et al*., 2001). Consequently, events have typically matured by the winter (JJA) prior to kauri breaking dormancy, then persist throughout the growing season, creating the opportunity for a relatively extended kauri response window, from JJA prior to growth, through to MAM. However, the fact that less than 20% of the annual growth ring is laid down after February suggests that the latter part of the window is likely to be less important, in terms of total ring-width signal.

The seasonal composite mapping results of Fowler (2005) and the K200 - SOI response function results (Figure 5(C)) are consistent with the above interpretation. Fowler found that wide and narrow tree rings tend to be associated with discernable ENSO-like MSLP anomaly patterns from the autumn prior to the growing season (MAM-1) through to the end of the growing season (MAM), with the strongest anomaly patterns in the middle three seasons (JJA-1, SON, DJF). These are also the peak correlation seasons (Figure 5(C)). The strength of the prior austral winter relationships may reflect site pre-conditioning (e.g. soil water or soil temperature). The fact that Fowler (2005) detected no discernable ENSO-like signal after MAM suggests that the declining negative correlations after the growing season in Figure 5 (JJA to JJA + 1) are probably statistical echoes of the growing season correlations, and are unlikely to represent additional information which may be useful for ENSO reconstruction.

The above results, and additional monthly response function analyses (not shown), indicate that the strongest 3, 6, 9, and 12 month ENSO signals in K200 are: SON ($R = -0.45$), SONDJF ($R = -0.48$), JJASONDJF ($R = -0.45$), and JASONDJFMAMJ ($R = -0.49$, Figure 8(A)). Calendar year relationships are weaker, due to ENSO impacts being spread across two years.

4.3. Relative importance of ENSO east and west poles

As previously noted, the New Zealand teleconnection to ENSO is SO-related and strongly linked to the western SO pole. It is therefore a reasonable expectation that the ENSO signal in kauri may be west-pole biased. MSLP composite mapping (Figure 6; Fowler, 2005) confirms this (stronger agreement in western than eastern MSLP anomaly spatial patterns). West-pole bias is further confirmed by the higher correlations of K200 with Darwin than with Tahiti MSLP through most of the growing season (Figure 7).

4.4. Relative sensitivity to El Niño and La Niña events

The weaker SO east-pole relationships noted above are primarily associated with narrow tree-ring composites (Figure 6(D)). A possible consequence is that kauri's ENSO signal may have an El Niño bias. This would not be surprising, given non-linearities in the ENSO teleconnection to New Zealand climate, related to MSLP fields and to local surface air temperature and precipitation (Mullan, 1996). Moreover, Jiang *et al*. (2004) note that changes in the frequency of synoptic weather types are more pronounced in El Niño than in La Niña years. To investigate this we constructed the contingency table shown in Figure 8(E) from quintile-partitioned K200 and mean July–June SOI data (Figure 8(B)). The results reveal strong similarities in the impact of El Niño and La Niña events, in terms of the frequency of wide and narrow kauri tree rings. For example, using one quintile definitions of ENSO events and wide and narrow tree rings (bold numbers in Figure 8(E)), El Niños and wide tree rings coincide 13 times, only marginally higher than the 12 coincidences of La Niñas and narrow rings. Relaxing the definitions to two quintiles (boxes in Figure 8(E)) also gives near-identical results. Given that the number of 'misassociations' of low (high) SOI with narrow (wide) rings is also very similar, these results suggest that any El Niño bias in K200 is likely to be small.

4.5. Relative sensitivity to the magnitude of ENSO events

Based on intensification of ENSO-like MSLP anomaly patterns associated with more extreme tree rings, Fowler (2005) concluded that kauri is sensitive to the magnitude of ENSO events. This is consistent with the linear relationship between K200 and the SOI (Figure 8(B)), but the results of the quintile partitioning analysis indicate that the interpretation may be too simplistic. Figure 8(C) shows: a) strong contrast between K200 Q1 and Q5 results; b) relative insensitivity in the frequency relationships across the middle three quintiles, and; c) abrupt transitions between Q1 and Q2, and between Q5 and Q4. Collectively, these suggest that the kauri growth response is primarily ENSO-event based and that the middle 60%

DOI: 10.1002/joc

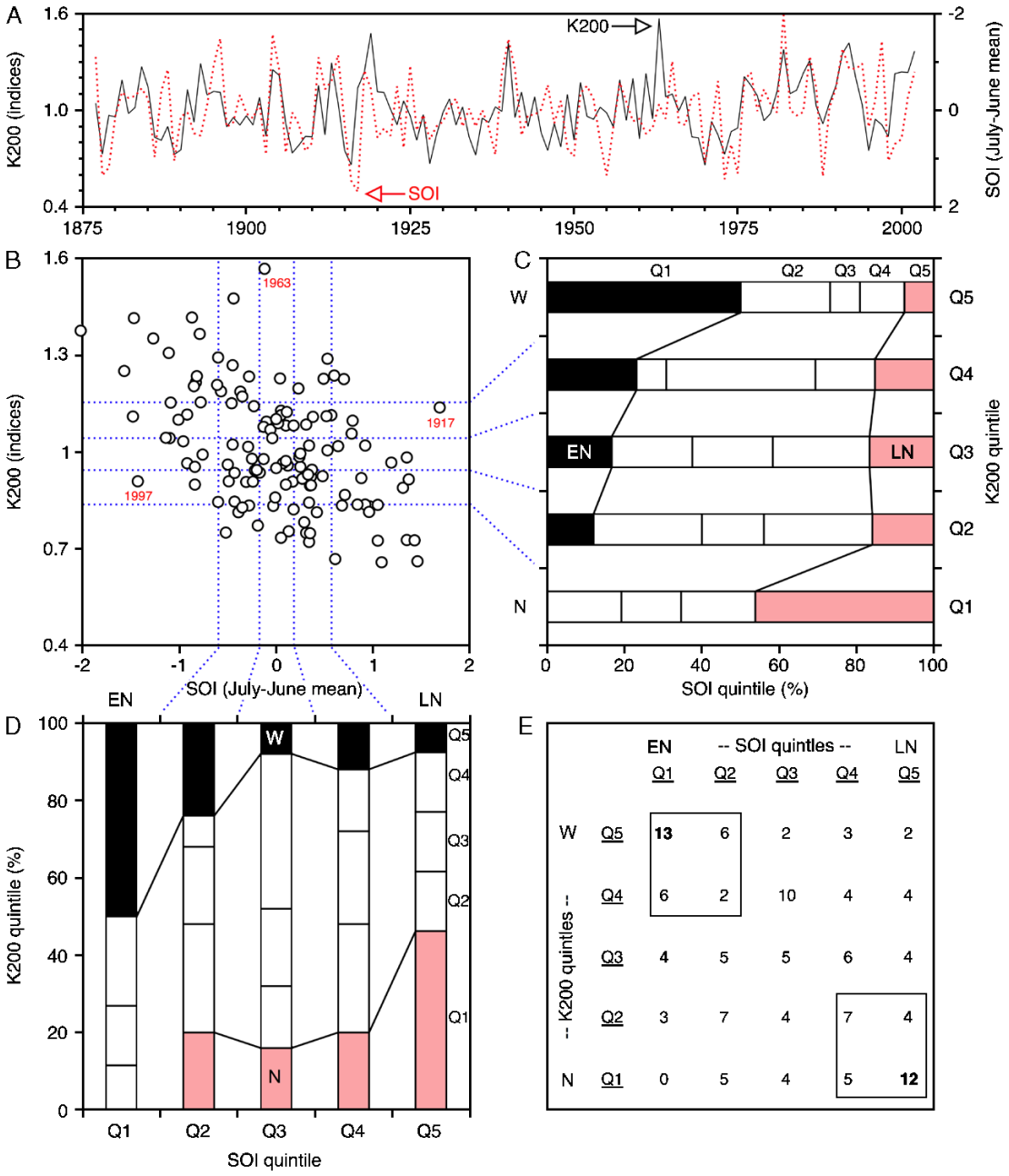

Figure 8. Relationship between K200 tree-ring indices and mean July–June SOI (1876–2002). A: time series plots (SOI inverted). Tree-ring indices are ratios about a mean of one (see Section 2.1). SOI is in standard deviation units about a mean of zero. B: scattergram with quintile partitions (dotted lines). Selected outliers are labelled with their start year (following the Southern Hemisphere convention for tree-ring dating). E: contingency table of the quintile-partitioned data, with each number associated with one of the 25 quintile-defined zones shown in B. C: Graphical presentation of the frequency counts in E, showing relative co-occurrence of SOI and K200 quintiles. Each bar in Panel C is associated with one of the K200 quintiles in Panel B, denoted by linking dotted lines and labelled 'Q1' through 'Q5' on the right axis. Each bar is divided according to the relative frequency of SOI quintiles co-occuring with that K200 quintile. D: same as C, but with each bar associated with one SOI quintile and divided according to K200 quintiles. For clarity, SOI Q1 is labelled El Niño (EN), SOI Q5 is labelled La Niña (LN), K200 Q1 is labelled narrow (N), and K200 Q5 is labelled wide (W). This figure is available in colour online at www.interscience.wiley.com/ijoc

of tree-ring indices (K200 Q2, Q3, Q4) contain little information about the probability of occurrence of an ENSO event.

4.6. Reliability of ENSO event registration

Quintile-based partitioning was also used to assess the reliability of kauri as an ENSO proxy, by quantifying the proportion of ENSO 'phases' (Q1–Q2, Q4–Q5) and 'events' (Q1, Q5) captured and misassociated in K200. A chi-square test of the contingency table (Figure 8(E)) indicates a statistically significant overall relationship ($p < 0.001$), and Figure 8(C) indicates near-symmetry in terms of ENSO registration in wide and narrow tree rings. Of the 52 widest tree rings (Q4, Q5), 52% are ENSO negative years (SOI Q1, Q2), 23% are neutral years (SOI Q3), and 25% are positive years (SOI Q4, Q5). Results

DOI: 10.1002/joc

for narrow rings are opposite but proportionately similar. Restricting the analysis to ENSO events (SOI Q1, Q5) slightly weakens the event strike rate to 46–50% (higher value for El Niños), but also significantly reduces the proportion of opposite associations to 0–8% (lower value for La Niñas).

The 3 years labelled in Figure 8(B) are significant outliers from the generic kauri-ENSO relationship. Two of the strongest ENSO events on record (1917, 1997) were respectively associated with moderately wide and narrow kauri tree rings (opposite in direction to expected) while the very wide 1963 tree ring did not coincide with a strong El Niño. These misassociations may relate to a 'breakdown' in the normal teleconnection between ENSO and local climate, and/or to idiosyncratic kauri growth response. To investigate this, prevailing climate conditions were reviewed for each outlier year (Table II), supplemented by inspection of MSLP and SST maps in Allan *et al*. (1996).

The SOI (July–June mean) was positive from May 1916, peaked through 1917, and persisted into May 1918. SST anomaly maps (Allan *et al*., 1996) indicate that New Zealand was surrounded by a continental-scale pool of water about 0.4 °C warmer than normal throughout that period. This warm pool was contiguous with comparable SST anomalies north of Australia throughout 1916, but the latter dissipated during the first half of 1917, and negative SST anomalies were in place by the end of the year. Consequently, for all of 1917 (especially the latter half) the main south Pacific SST anomaly contrast was between the cold eastern Pacific and warm pool anomalies centred over New Zealand. Dissipation of positive warm pool anomalies north of Australia coincided with a weakening of western ENSO pole pressure anomalies (Allan *et al*., 1996). Notwithstanding that the SOI remained strongly positive throughout 1917–1918 growth year, the MSLP and SST features of the western ENSO pole were not characteristic of a La Niña event, although local climate conditions (warm and wet) were, especially early in the growing season (Table II). It is plausible that the misassociation of a wider than normal kauri tree ring in 1917 relates to non-La Niña processes being responsible for the warm-wet conditions (presumably the large warm pool surrounding New Zealand). Or it may be related (in some unknown way) to the coupling of two La Niña years. Although the 1917 tree ring is the most extreme case, similar situations occurred in 1878 and 1979, and again in 1998 and 1999 (Figure 8).

The SOI for 1963–1964 was in the middle quintile (Figure 8(B)), supposedly indicative of near-neutral ENSO. However, this is somewhat misleading, since the July–June window covers a change from negative to positive values of the SOI in February 1964. Indeed, 1963 is often identified as a weak El Niño in ENSO event lists (e.g. Mullan, 1995). Accepting that 1963 was an El Niño year and that the index is deficient in this instance eliminates the false positive problem, but a conundrum remains in the coincidence of a relatively weak El Niño with the widest ring in over 400 years. A partial explanation is the fact that the 1963 El Niño and its associated local climate impacts peaked in SON (Table II), the season of greatest kauri growth (Fowler *et al*., 2005). Moreover, the local climate anomalies (cool and very dry) were relatively large for the size of the El Niño. A wide ring in 1963 is therefore no surprise, but there remains no convincing explanation for it being the widest.

The SOI was negative from March 1997 until May 1998. It was in the lowest seasonal decile throughout, making 1997–1998 one of the strongest El Niños of modern times. A wide kauri tree ring would therefore have been expected. NOAA SST analyses (www.elnino.noaa.gov) indicate very large SST anomalies in the eastern Pacific, but weaker and spatially less organized patterns in the west. Significantly, for the New Zealand teleconnection region, the Tasman Sea was relatively warm through most of this period, and the kauri growth region was surrounded by a warm pool from February 1998. Seasonal climate statistics (Table II) are contrary to expected El Niño relationships. The peak kauri growth season (SON) was warm and very wet, and was followed by dry and very warm DJF and MAM. Soil water conditions were unexceptional. Kauri growth was consistent with these La Niña-like conditions, suggesting that the absence of a wide kauri tree ring in 1997 is a relatively clear case of breakdown of normal teleconnection patterns.

Table II. Summary of climate conditions associated with three outlier years (1917, 1963, 1997) for the five-season kauri response window (Section 4.2). Plus (minus) symbols indicate positive (negative) anomalies for tabled variables and the number of symbols shows the size of the anomaly (1 = outside middle quintile, 2 = upper/lower quartile, 3 = upper/lower decile). Statistics calculated for the common period 1901–1997. Climate data are described in Section 2.2.

	MAM-1	JJA-1	SON	DJF	MAM
1917–18					
SOI	+++	+++	+++	+++	++
Tmean		++	+		+
Precip.	+++	+++	+		
Soil water	+++	+++	++		+
1963–64					
SOI	++	−	−−	−	++
Tmean	−			−	−
Precip.	−	−	−−−	−−	−
Soil water	−	−	−−	−−	−−
1997–98					
SOI	−−−	−−−	−−−	−−−	−−−
Tmean	+	−	++	+++	+++
Precip.		−	+++	−	−−
Soil water	−		+	−	−

4.7. Spectral signature

Instrumental ENSO indices have a well known spectral signature (Allan, 2000). Power is focused in a

DOI: 10.1002/joc

2–10 year periodicity band, with large decadal-scale variability in the power distribution within this band (Kestin *et al*., 1998). Notable decadal-multidecadal fluctuations in ENSO characteristics have also been identified (Torrence and Compo, 1998; Allan, 2000). Because ENSO's spectral signature is well known, it is common for the spectral signature of ENSO proxies to be compared to it, to assess proxy quality and identify which of ENSO's frequency components the proxy may have skill in reconstructing (e.g. D'Arrigo *et al*., 2005).

Wavelet analyses (Torrence and Compo, 1998) of the SOI, Tahiti MSLP, Darwin MSLP, and K200 indices are shown in Figure 9, all for the period 1876–2002. For consistency with the tree-ring indices, the SOI and the two MSLP analyses were run on July–June mean values. Results for the SOI (Figure 9(A)) are similar to those obtained using monthly data by Torrence and Webster (1999). Comparison of the Tahiti and Darwin MSLP wavelet plots shows broad similarities (e.g. significant power in the 2–10 year periodicity band, peaking near either end of the 20th century), but also some differences (e.g. pre-1900 power in the 8–16 year band is unique to Tahiti and multi-decadal features appear to carry more power in the case of Darwin). It follows that some features in the SOI plot carry unequal contributions from the respective poles of the SO.

Comparison of the K200 wavelet plot (Figure 9(F)) with those for the SOI, Tahiti, and Darwin (Figure 9(A), (B), (C)) indicates much less power carried by kauri at 2–8 year periodicities. Although a focus of power at less than eight year periodicity is apparent at either end of the 20th century, consistent with the SOI, most power is focused at decadal and multi-decadal frequencies (especially 8–16 and, largely separately, at 16–32 years). Most of the low frequency features in Figure 9(F) have an echo in the SOI and/or one of the MSLP plots. For example, the 8–16 year power peak in the late 19th century, which evolves to a 4–8 year peak by the 1910s, is present in the SOI (the former part carried predominantly by Tahiti). Other similarities include: the late 20th century K200 power peak at about 6–10 years (present in the SOI and also carried mostly by Tahiti); the extension of this power peak through to the broad 16–32 year power centred in the 1960s (present in the SOI but predominantly a Darwin feature); and the concentration of low frequency power in the latter half of the record. A notable discrepancy is the absence of the 4–8 year periodicity power peak straddling the middle of the 20th century, evident in all three SO-related plots.

Given the strength of the relationship between kauri tree rings and ENSO previously identified, the weakness of the spectral signature in K200 in the 2–8 year periodicity band and the concentration of power at decadal to inter-decadal periodicities is curious. One possible explanation is that kauri's ENSO event capture skill is too low to preserve high frequency structure, but is sufficient to retain the low frequency signal. We know from Section 4.6 that about half of El Niño (La

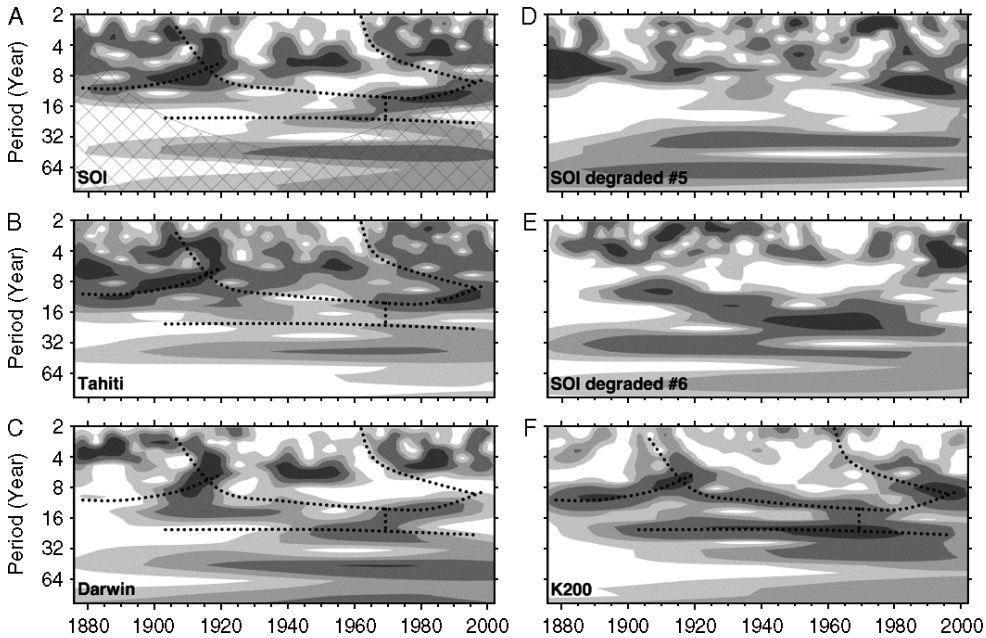

Figure 9. Comparative Morlet wavelet analysis of ENSO indices and K200 using the method of Torrence and Compo (1998). For consistency, all analyses are for the period 1876–2002 using annual data (tree-ring indices for K200, July–June mean for the SOI and Tahiti and Darwin MSLP), using zero padding to reduce wraparound effects (Torrence and Webster, 1999). Shading shows 75, 50, 25, and 5% of the wavelet power. The cross-hatched region in Panel A (common to all panels but omitted for clarity) is the 'cone of influence', where zero padding has reduced the variance. Panels D and E are analyses for 'degraded' versions of the SOI, reflecting the characteristics of ENSO event registration in K200 (see text for details). Dotted lines in Panel F trace key spectral features in the K200 analysis. These are superimposed onto Panels A-C to assist comparison. Statistically significant patterns, at the 10% level using a red noise background spectrum, are nearly idententical to the 5% power band (darkest shading) in all cases. Wavelet analyses were run using the Torrence and Compo (1998) online wavelet toolkit (http://paos.colorado.edu/research/wavelets).

DOI: 10.1002/joc

Niña) events are captured by upper (lower) quintile K200 indices, and that about half of the tree rings in those quintiles are false positives of some form (but with few event reversals). ENSO event reconstruction based on K200 upper and lower quintiles would therefore miss half the events and substitute an equal number at incorrect years. (This is not as bad as it might seem, as about half of the missed events and false positives involve 'shifts' between the adjacent quintiles (Q1 $\Leftrightarrow$ Q2, Q5 $\Leftrightarrow$ Q4)). If the missed events and false positives were randomly distributed in time, periods of high ENSO event frequency may be preserved (similar numbers of missed events and false positives), even though the high frequency signal is lost.

To test the above we 'degraded' the SOI in accordance with the K200 quintile probabilities in Figure 8(D). For example, in the case of a La Niña year (SOI Q5), the probabilities of the year being assigned to Q1, Q2, Q3, Q4, and Q5 were 0.08, 0.15, 0.15, 0.15, and 0.46 respectively (K200 quintile probabilities in reverse order). When assigned to an SOI quintile (even the same quintile) the SOI value for the year was randomly drawn (with replacement) from the SOI values associated with that quintile. Multiple 1876–2002 times series were then generated, and the first 10 with roughly equal numbers (22–30) in the revised 'quintiles' and a correlation with the non-degraded SOI similar to that between the SOI and K200 ($0.40 < R < 0.52$) were retained. Wavelet analysis of these degraded SOI series (e.g. Figure 9(D) and (E)) indicates high sensitivity of the high frequency signal to degradation analogous to ENSO event registration in kauri tree rings. Power in the 2–8 year periodicity band was generally weaker and there were some substantial changes in the location of apparent cyclicity peaks. Lower frequency features were better retained (e.g. Figure 9(D) and (E)), but most plots showed evidence of substantial change. A few experiments (e.g. Figure 9(E)) produced wavelets patterns with decadal-multidecadal features similar to those shown for K200 (Figure 9(F)).

4.8. Stationarity of relationships

Stationarity is a known issue associated with ENSO, even within the tropical core zone. For example, Allan *et al.* (1996) noted decadal-multidecadal waxing and waning of the robustness of ENSO and of the stability of associated teleconnections, including significant changes in the relationship between Darwin and Tahiti MSLP. They also identified significant fluctuations in the correlation between Darwin and global MSLP fields and identified 1921–1941 as a period of reduced ENSO activity. Torrance and Webster (1999) identified 1920–1960 as a period of relative ENSO quiescence. Similarly, Trenberth and Stepaniak (2001) noted substantial change in the evolution of El Niño events from the mid-1970s, from westward to eastward propagating SST anomalies, associated with an abrupt Pacific climate shift. Since the character of ENSO events, and therefore extra-tropical teleconnections, are significantly influenced by tropical SSTs (Trenberth and Stepaniak, 2001), multi-decadal changes in relationships are likely, especially at more distant locations.

Mullan (1995) investigated the stationarity of relationships between the SO and New Zealand climate, by regressing the SOI against surface air temperature and precipitation at 44 sites, then comparing the regression results (e.g. regression line slopes) for different time periods. Mullan identified 1950 as a critical demarcation point and 1928–1949 as a period of weaker relationships (in all seasons). For the kauri growth region, key differences in the 1928–1949 period (compared to 1950–1989) are: absence of strong relationships with SON precipitation and JJA temperature; reversal of the relationship with DJF temperature; and a strengthening of the DJF precipitation relationship. In the context of the statistical relationships between K200 and climate (Figure 5), such changes would be expected to weaken the relationship between K200 and the SOI, raising the possibility of a stationarity issue when using kauri as an ENSO proxy. This was investigated using MSLP composite mapping and evolutive response function analysis.

Figure 10 shows gridded MSLP anomalies associated with wide and narrow tree rings for 1876–1910, 1911–1950, and 1951–1994. The number of years in each composite varies, depending on the variance and decadal-scale trend in K200 (Figure 8(A)), but the $\pm 10\%$ tree-ring index thresholds used results in at least 9 years in each composite. Near-reciprocal patterns are evident for the late 20th century, similar to those shown for ENSO in Figure 6(A) and (C), although the pattern for narrow rings (Figure 10(F)) has eastern Pacific peak positive MSLP anomalies displaced much further south than the La Niña composite map (Figure 6(C)). Spatial patterns are similar for 1876–1910, especially over Australia and the Indonesian archipelago, but pattern strength is weaker, although the latter (and the greater extent of white space) may simply reflect infilling of early period missing data with climatology in the compilation of the GMSLP2.1f data set (Basnett and Parker, 1997).

Notwithstanding the above caveat regarding the effects of infilling missing data, the 1911–1950 MSLP composite maps in Figure 10 clearly differ from those for the other two periods. The patterns are generally weaker than those for 1876–1910, when reduced infilling of missing data would be expected to result in stronger relationships. They also show less spatial coherence, especially in the eastern Pacific, including reversals of sign over the Americas. Anomalies over Australia are still evident, although somewhat reduced in spatial extent, but peak anomalies are now centred over eastern Australia and the western Tasman Sea, rather than northern Australia and Indonesia. Note that identification of 1911–1950 as anomalous for kauri-MSLP relationships is consistent with the identification of the mid 20th century as a period of less robust ENSO activity (Allan *et al.*, 1996; Trenberth and Stepaniak, 2001) and of weaker relationships between the SO and New Zealand climate.

DOI: 10.1002/joc

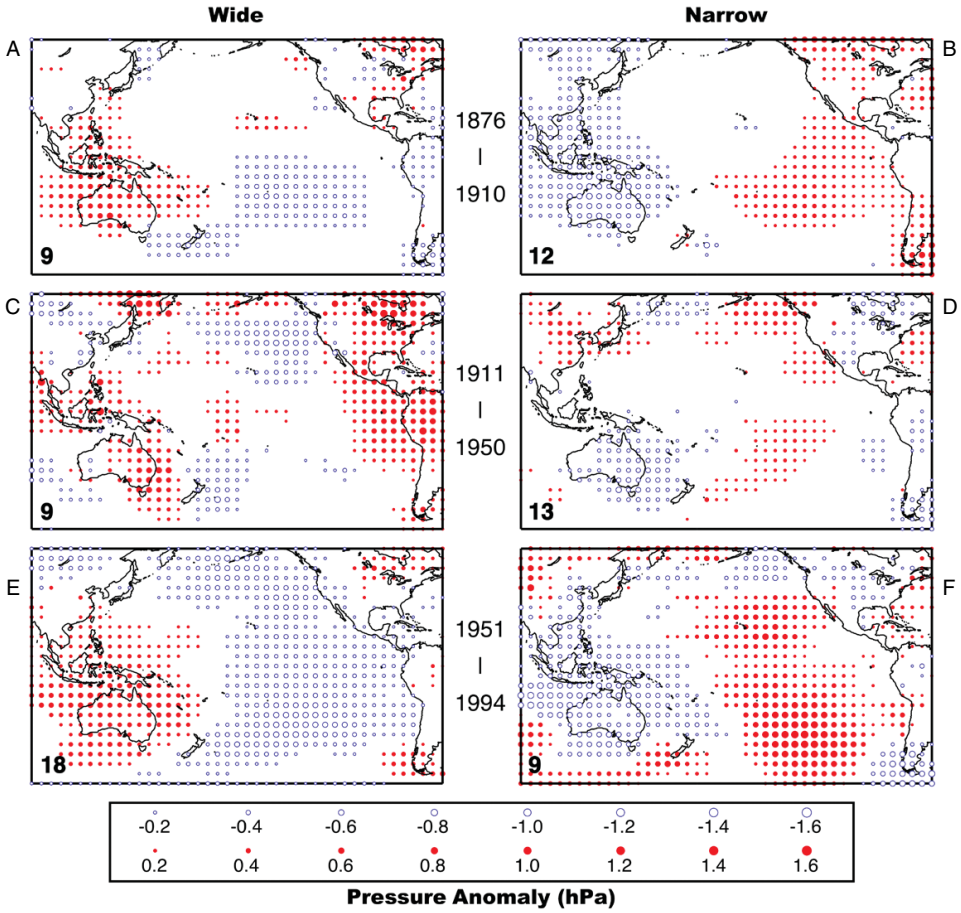

Figure 10. July-to-June MSLP anomaly composite maps for wide (1.1<K200) and narrow (K200<0.9) tree rings, for three time periods. The number of years in each composite is indicated by the number in the bottom-left of each panel. Anomalies were calculated relative to gridded MSLP for each labelled time period. This figure is available in colour online at www.interscience.wiley.com/ijoc

Evolutive correlation response function analysis of the relationship between K200 and the SOI is presented in Figure 11(A), for lags of up to four years through to the last season in which growth may occur (JJA). A horizontal line through a row in Figure 11(A) is analogous to Figure 5, but for a 31 year subset of the data, and with *R* symbol-coded. Stationary relationships are indicated by columns of circles or dots of similar size and colour. The most striking such pattern is the four seasons of persistent negative correlations from autumn immediately prior to growth (MAM-1) through to the concurrent summer (DJF), although the MAM-1 relationship is weak. In contrast, evolving correlations at lags of 2–4 years show clear evidence of non-stationarity. Correlations from DJF-4 through to MAM-2 are consistently positive and relatively strong, up to the 31 years centred on 1930, after which temporal patterns are less coherent, relationships generally weaken, and in some cases reverse in sign. A further possible sign of non-stationarity is the fact that, although correlations for MAM and JJA are relatively strong in the first and last few decades, they are very weak (and sometimes reversed) for several decades centred on about 1950. The Monte Carlo simulations of Van Oldenborgh and Burgers (2005) indicate that such decadal-scale variation in running correlations could be due to chance, but the fact that the beginning of the low *R* period coincides with the clear evidence of non-stationarity in the case of lagged relationships suggests that this may not be a chance occurrence.

The abrupt change in relationships in Figure 11(A) between 1930 and 1935 is a result of the 31 year correlation window exiting the 1910s, a decade of conjoint high kauri and SOI variance and relatively strong agreement between them (Figure 8(A)). This explains the significant declines in variance between these dates for both K200 (Figure 11(D)) and the SOI (Figure 11(E)) and is consistent with the start of the mid 20th century ENSO-quiescent period previously identified. K200 and the SOI then enter variance troughs, with near-synchronous lower limits about 1940. MAM and JJA relationships are weakest during this time. Correlations between K200 and growing season SOI are strong again in the last few decades of the 20th century, coincident with conjoint high variance in both time series. At this time the two series also have significant and opposite decadal-scale trends (Figure 11(B) and (C)). This amplifies negative correlations from MAM-1 on, and may partly explain the absence of consistent positive lag correlations.

DOI: 10.1002/joc

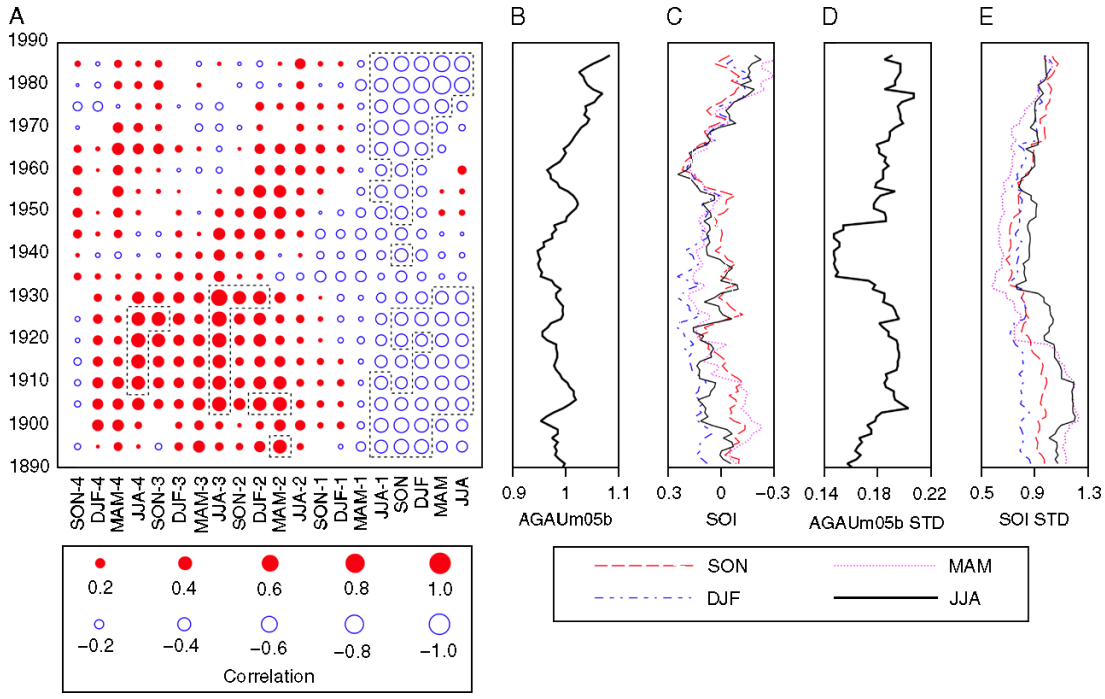

Figure 11. SOI-K200 evolutive response function (Panel A). Dots (circles) indicate positive (negative) correlations for a sliding 31 year window (plotted against the middle year) in five year steps. Symbol area is proportional to the correlation and significant correlations ($p < 0.05$) are enclosed by dashed lines. Right-side panels are mean and standard deviation statistics for K200 (B, D) and for seasonal means of the SOI (C, E), also for a sliding 31 year window, but in one year steps. X-axis reversed in C. This figure is available in colour online at www.interscience.wiley.com/ijoc

5. Discussion

5.1. The kauri – ENSO relationship

Evidence presented in Section 3.1 indicates that kauri site chronologies carry a common regional-scale forcing signal, with one exception (MOEH). Based on this, and similar conclusions derived from principal components analysis (Fowler *et al*., 2004), kauri master chronologies were built by pooling data for all trees (except MOEH). Sections 3.2 and 3.3 show that the regional-scale forcing signal is amplified in the master chronologies and that ENSO is a significant component of that forcing.

Based on several lines of evidence (Section 4.2), a five season kauri response window to ENSO was deduced, extending from the austral autumn prior to growth initiation (probably in September) through to autumn at the end of the growing season. Relationships are strongest over the three middle seasons (JJA-1, SON, DJF). Extension of analyses to different ENSO indices, and to Tahiti and Darwin MSLP indicates that, within the five-season response window, kauri tree-ring indices:

(1) are more strongly correlated to SO-related indices than to Niño3.4 SSTs (Section 4.1);
(2) are slightly biased, in terms of signal strength, towards the western pole of the SO (Section 4.3), and;
(3) carry a slightly stronger and more consistent signal of El Niño than La Niña events (Sections 4.4, 4.6).

All three findings are consistent with known ENSO teleconnection relationships to New Zealand.

5.2. ENSO reconstruction potential

It is clear from Figure 7 that kauri sensitivity to ENSO is concentrated within the five-season response window identified above. Persistent negative correlations (declining in significance) for seasons after MAM probably reflect ENSO persistence, carrying little or no additional information. Similarly, persistent weak positive correlations at lags of 2–4 years may be statistical artefacts associated with ENSO auto-correlation. Given the weakness of the relationships and stationarity issues associated with the 2–4 year lag correlations (Section 4.8), we conclude that the reconstruction potential of kauri is largely confined to the ENSO state immediately prior to and during the growing season. This conclusion differs from that reached by Fowler *et al*. (2000), who argued, based on stronger 2 year lag correlations, that lag relationships may have reconstruction potential.

The five-season response window is mostly determined by statistical relationships. It is plausible that kauri's growth response to ENSO is actually more restricted in time, and that the (statistical) window is wider simply because of the typical life cycle of ENSO events. For instance, if kauri were only affected by ENSO during SON and DJF, we would nevertheless expect only slightly weaker correlations with the seasons either side, because ENSO events are typically mature by JJA-1 and persist through MAM. Of course it is also possible that correlations with MAM-1, and especially JJA-1, reflect real biophysical effects associated with tree or site preconditioning (e.g. soil water/temperature). Likewise, the weaker MAM correlations may reflect ongoing ENSO

DOI: 10.1002/joc

impacts, but at a time of lower sensitivity because little of the tree ring is laid down in MAM (Fowler *et al*., 2005). Current knowledge of the kauri growth response to evolving environmental variables (e.g. the importance of soil water/temperature to growth initiation) is not sufficient to resolve such questions. Recent work on kauri – environment relationships by Fowler *et al*. (2005) has refined understanding, and continuing research is expected to help tease out relationships currently hidden in the scatter of Figure 8(B), and to explain some of the anomalies identified in Section 4.6. It is even possible that some of these anomalies, such as the weak kauri response to the second of coupled La Niña years, may be a source of additional information, rather than simply statistical noise.

Incomplete knowledge of kauri – environment relationships does not preclude using kauri tree rings for ENSO reconstruction. Indeed, multi-variate statistical transfer functions currently popular in ENSO reconstruction work (e.g. Mann *et al*., 2000; D'Arrigo *et al*., 2005) are mathematical constructs, derived from proxies 'reduced' to simple numerical time series. In the context of such statistical transfer functions, our results indicate that kauri has most potential for ENSO reconstruction from mid-year through to the start of the next. Calendar-year reconstruction is not ideal and even a 12-month period from mid-year to mid-year (as used here) is somewhat problematic because it will sometimes encompass an ENSO phase change, as in 1963–1964 (Section 4.5).

The overall relationship between kauri and the SOI is statistically significant. However, it is dominated by associations between ENSO events and wide and narrow tree rings, with only a weak relationship across the middle three quintiles of the SOI. This means that kauri tree-ring widths carry useful information about ENSO event occurrence, but tell us little about the event magnitude. Moreover, only about 50% of El Niños (La Niñas) coincide with wide (narrow) tree rings (Figure 8). At 2.5 times greater than what would be expected by chance this represents useful skill, particularly when combined with the fact that opposite associations (e.g. wide rings associated with La Niñas) are rare, but it is probably too low a 'strike rate' to warrant stand-alone reconstruction of ENSO events. More usefully, kauri could be incorporated into multi-proxy ENSO research. This includes both multi-variate statistical approaches (e.g. Mann *et al*., 2000), and event list compilation (e.g. Whetton and Rutherfurd, 1994). Including kauri would have particular merit because of its location in the data-deficient Southern Hemisphere, and its stronger relationship to the under-represented western pole of the SO.

The limitation of kauri for stand-alone reconstruction of ENSO events is reinforced by the lack of power in the 2–8 year spectral band (Figure 9(F)). This is probably partly a consequence of the sensitivity of the high frequency signal to missed events and false positives in the kauri proxy. Decadal-scale periodicity features are better preserved and it is noteworthy that concentration of spectral power early and late in the 20th century is consistent with the SOI (although at lower frequencies). It is also consistent with expectations, since the early and late 20th century are periods of robust ENSO activity (Section 4.8). Because kauri growth carries a strong signal of regional-scale forcing, and ENSO is a significant forcing contributor, we would expect to see greater power at ENSO frequencies during ENSO-active periods. The associated stronger coupling between kauri and ENSO during these periods is evident in the time series plots (Figure 8(A)) and is clearly signalled by stronger correlations with the SOI during the growing season (Figure 11(A)). Robust ENSO periods are characterized by high ENSO variance (Figure 11(E)), again coinciding with periods of higher K200 variance (Figure 11(D)). This suggests that evolving kauri time series variance (for a moving window) may be a useful index of multi-decadal variability in ENSO strength.

Most of the analyses presented here used K200. This is because K200-SOI statistical relationships are only marginally weaker than K20-SOI relationships, especially over the critical five-season response window (Figure 5(C)), and our presumption that retention of multi-decadal signal is inherently desirable. In the context of kauri – ENSO relationships, retention of time-series trend has four noteworthy implications. First, trend alters (e.g. via partitioning analysis) the association of wide/narrow rings with ENSO events. Most importantly, it increases (decreases) the representation of late 20th century wide (narrow) rings in the upper (lower) quintiles. It also changes event rankings, relative to K20. Second, wavelet periodicity features above about 16 years (Figure 9(F)) are essentially a product of the retained trend. Third, trend increases variance in a time series window (e.g. the late 20th century variance peak in K200 (Figure 11(D))). Fourth, retaining trend permits investigation of multi-decadal periods of above and below average kauri growth, possibly related to protracted El Niño or La Niña states. If multi-decadal trend in K200 is ENSO-forced, then each of these four points represents useful additional information. Otherwise, trend represents unwanted bias (associated with some other unknown forcing factor), retention of which would contaminate the ENSO signal.

The fact that observed trends in the tree-ring indices are consistent with event-based relationships supports the contention that K200 trend is ENSO-related. Because wide kauri rings are strongly related to El Niños, the trend towards more intense and (especially) more frequent El Niños in the late 20th century would be expected to result in the observed increase in the number of wide rings, and therefore an elevated late 20th century mean. In contrast, the ENSO-robust period in the early 20th century is not characterized by a change in the relative proportions of El Niño and La Niña events. The associated K200 near-normal mean and high variance (Figure 11(B) and (D)) are again consistent with ENSO-forcing of trend. Based

DOI: 10.1002/joc

on this consistency of relationships, we conclude that decadal-scale trends in mean kauri tree-ring indices *may* be a proxy for the relative mix of El Niño or La Niña events. However, we acknowledge that the instrumental data is insufficient to warrant definitive conclusions in this regard and that alternative explanations of such trends are possible.

D'Arrigo *et al*. (2005) produced what is probably the best proxy reconstruction of ENSO yet published, based on subtropical North American tree rings. Spectral analysis of the proxy reconstruction of Niño3 SSTs indicated good resolution of ENSO variability in the 2–8 year band, but no significant power at lower frequencies (D'Arrigo *et al*., 2005). This is in marked contrast to kauri, which has power peaks at decadal- to multi-decadal time periods. It is noteworthy in this regard that the D'Arrigo *et al*. (2005) reconstruction is for ENSO eastern pole SSTs, whereas kauri growth response is dominated by the western pole and the SO. Also, as previously noted, there is some indication that the western SO pole carries greater lower frequency power than the eastern pole. Given the contrasts between D'Arrigo *et al*. (2005) and kauri (SST *vs* SO, east *vs* west, high frequency *vs* low frequency), future research combining the proxies may have considerable potential.

5.3. Stationarity issues

As noted in the opening paragraph of this paper, two key uncertainties related to ENSO are the stationarity of 20th century teleconnections and decadal through millennial evolution of ENSO's character. In terms of ENSO reconstruction from proxies, these two uncertainties are closely entwined. Clearly, if the relationship between a proxy and ENSO is non-stationary, reconstruction of ENSO's evolving character using that proxy will be flawed. The problem is most acute in the case of ENSO reconstruction from single proxies from teleconnection regions outside ENSO's tropical core zone, because more distant teleconnections are likely to be weaker and more variable, and because single-proxy non-stationarities cannot be identified by reference to other ENSO-sensitive proxies.

Although the far-north of New Zealand is 4000–5000 km distant from Tahiti and Darwin, it nevertheless has a high-order connection to the SO through MSLP fields associated with both El Niño and La Niña events (Figure 6). It is because New Zealand lies on the cusp between positive and negative MSLP anomaly fields that ENSO events significantly affect prevailing winds, with associated impacts on local climate. Fowler (2005) showed that larger ENSO events are associated with more intense MSLP anomalies, but that spatial patterns over New Zealand remain essentially the same, indicating that similar causal mechanisms probably operate throughout the range of ENSO events. This is consistent with the findings of Jiang *et al*. (2004) who found stationarity in the *characteristics* of synoptic situations over New Zealand associated with different SOI phases, with ENSO impacts experienced through changes in frequency. Also important is the stationarity analysis of gridded reconstructed global surface air temperature by Mann *et al*. (2000), their Figure 10.19, which showed the New Zealand region to have one of the strongest, spatially coherent, and consistent relationships (negative correlation) with their reconstructed Niño3 index (AD 1651–1901). This includes the 1801–1850 period, identified by Mann *et al*. (2000) as having global teleconnection patterns inconsistent with other periods. However, one caveat to add to this benign assessment of the stationarity of ENSO teleconnections over New Zealand is that Mullan (1995) identified a different pattern for 1928–1949. He acknowledged that this may be associated with a stationarity issue with ENSO, rather than with the teleconnection, but also suggested that it might relate to regional changes in atmospheric circulation. Salinger and Mullan (1999) identified 1950 and 1975 as regional atmospheric circulation change points.

Fowler (2005) found some evidence of non-stationary in the MSLP anomaly fields associated with wide and (especially) narrow kauri tree rings, including an apparent breakdown of the relationship between narrow tree rings and MSLP anomalies in the late 20th century. However, the Fowler (2005) analysis was flawed because equal three-way splits of the data were used for each period investigated. Because of the late 20th century trend towards more El Niño events, several near-neutral ENSO years were included in the La Niña composite, with consequent weakening of the MSLP anomaly signal. Reanalysis here (Figure 10), using absolute kauri tree-ring thresholds ($\pm 10\%$) to partition the gridded MSLP data, indicates no major breakdown in late 20th century La Niña relationships. Rather, the important conclusion to be drawn from MSLP composite mapping is the weakness of 1911–1950 patterns (Figure 10(C) and (D)), coinciding with the previously identified periods of reduced ENSO activity (Section 4.8).

Explicit investigation of the stationarity of the kauri – SOI statistical relationships (Figure 11(A)) revealed non-stationary lag relationships. Growing season relationships are stationary, apart from the weakening of relationships in the mid-20th century, probably caused by reduced ENSO activity, and consistent with the composite mapping results. However, although there is no convincing evidence of multi-decadal non-stationarity in growing season ENSO-kauri teleconnections, analysis of anomaly years (Section 4.6) suggests that this is not the case on an event basis. For example, the 1997–1998 El Niño was associated with local climate conditions very different to the El Niño teleconnection norm. Kauri growth was consistent with the local conditions, rather than the SOI, resulting in a missed event. Similarly, the 1963 wide tree ring was consistent with strong El Niño-like conditions in the New Zealand region, especially early in the growing season. This indicates that breakdown of normal teleconnection patterns for some events is partly responsible for some of the missed events and false positives discussed in Section 4.6.

DOI: 10.1002/joc

6. Conclusions

Kauri tree rings carry a strong regional-scale climate signal, dominated by ENSO. Understanding of the physical processes is incomplete, but perturbation of regional atmospheric circulation by the SO (especially the western pole) clearly dominates. ENSO events change the relative frequency of different synoptic situations, with significant associated impacts on prevailing winds. The net effect is that El Niños (La Niñas) tend to be associated with cool-dry (warm-wet) climate anomalies in the kauri growth region and with wide (narrow) kauri tree rings. Kauri responds in a reciprocal manner to El Niño and La Niña events, but has a slightly stronger and more consistent relationship to El Niños.

We identify a five-season kauri response window, extending from the austral autumn prior to growth (MAM-1) through to the following autumn, with peak relationships in the middle three seasons (JJA-1, SON, DJF). Relationships within this response window appear to be stationary, apart from weaker relationships in the mid-20th century, coincident with less robust ENSO activity. There are also weak non-stationary lag relationships. Taking into account the strength of statistical relationships, stationarity issues, and the typical life-cycle of ENSO events, we conclude that kauri tree rings have greatest potential for ENSO reconstruction for multi-month blocks within the 9 months from June prior to growth through to February.

About half of wide (narrow) kauri tree rings (upper/lower quintiles) are associated with El Niño (La Niña) events. At 2.5 times chance, this represents useful skill, but it also means that half of ENSO events are missed and half of the wide and narrow tree rings are false positives (incorrectly interpreted as ENSO events). We judge this skill level to be insufficient to warrant stand alone ENSO reconstruction using kauri tree rings, but sufficient for kauri to be a valuable addition to multi-proxy ENSO research, especially given its geographical location. K200 is listed as an appendix to facilitate such work.

Notwithstanding kauri's limitations for stand-alone ENSO event reconstruction, our results suggest that the strength of the ENSO-kauri relationship is strong enough to preserve a signal of evolving ENSO robustness. This is shown by the similar time-evolving patterns in the SOI and K200 variance plots (Figure 11(D) and (E)). Since the relationship between K200 and ENSO appears to be stationary, it may therefore be feasible to reconstruct ENSO robustness from kauri tree rings alone. This is the subject of Part B of this research (Fowler, this issue).

Acknowledgements

Financial support for this research was provided by the New Zealand Foundation for Research, Science and Technology (FRST contract UOAX0011) and by the Royal Society of New Zealand (Marsden Fund grant UOA108). We thank the United Kingdom Meteorological Office (Hadley Centre) for access to the GMSLP2.1f data set, accessed through the British Atmospheric Data Centre. Tahiti and Darwin MSLP data and the SOI were obtained from the Australian Bureau of Meteorology web site. The homogenized Mangere climate data were kindly provided by Jim Salinger. Our thanks to the Department of Conservation, Waipoua Forest Trust, Te Iwi o Te Roroa, Water Care Services Ltd, and private landowners for access to the sites listed in Table I.

Appendix. Kauri Master Tree-Ring Chronology AGAUm05b

	Year									
Decade	0	1	2	3	4	5	6	7	8	9
1580	1.037	1.141	0.930	1.033	0.858	1.256	1.108	1.273	1.005	1.162
1590	1.130	1.330	1.174	1.070	1.174	1.056	1.170	0.984	0.834	0.984
1600	0.864	1.152	0.697	0.895	0.906	1.016	0.982	1.111	1.051	0.868
1610	1.125	0.924	1.014	1.014	0.794	0.876	0.878	1.090	1.080	1.077
1620	1.128	1.101	0.892	0.870	0.849	0.919	0.928	1.060	1.188	0.904
1630	0.995	1.015	0.863	0.839	0.897	0.731	0.939	0.877	0.880	0.908
1640	0.832	1.027	0.969	0.913	0.779	0.766	0.842	0.810	0.890	0.708
1650	1.008	0.895	0.865	1.018	0.684	1.049	0.792	1.065	0.876	1.079
1660	1.102	0.956	0.771	0.899	1.063	1.110	1.071	1.289	1.039	1.252
1670	1.123	1.235	1.104	1.115	1.175	1.047	1.194	1.002	0.804	1.021
1680	0.921	1.026	0.778	1.016	0.757	0.991	1.012	1.116	1.000	0.911
1690	0.821	1.063	0.955	0.953	1.297	1.139	1.144	1.157	1.122	0.987
1700	1.145	0.972	0.962	1.108	1.041	0.932	0.958	0.828	0.846	0.893
1710	1.011	1.094	1.012	0.962	1.078	0.872	1.034	1.025	0.967	1.164

(*continued overleaf*)

DOI: 10.1002/joc

(*Continued*)

Decade	Year									
	0	1	2	3	4	5	6	7	8	9
1720	1.035	1.057	0.942	1.069	0.621	0.888	1.024	0.914	1.085	0.959
1730	0.992	0.929	0.816	1.148	1.248	1.083	1.259	1.143	0.839	0.999
1740	0.769	0.905	1.148	0.839	1.141	0.762	1.237	1.250	1.072	1.030
1750	0.679	0.969	0.797	0.974	0.833	1.061	0.930	0.861	1.230	1.074
1760	0.898	1.015	0.930	0.928	0.852	0.843	0.821	0.823	0.978	1.097
1770	0.840	0.871	0.846	1.016	1.073	0.978	1.007	1.053	0.857	1.037
1780	0.875	1.042	1.030	0.778	1.075	1.037	1.164	0.863	1.204	0.918
1790	1.013	1.170	0.781	0.930	0.993	0.775	1.032	1.161	1.088	1.258
1800	0.963	0.975	0.884	0.993	0.842	0.813	1.019	1.036	0.942	1.256
1810	1.064	1.205	1.107	1.026	1.015	1.105	1.224	0.981	1.021	0.939
1820	1.081	0.956	1.112	0.942	0.974	0.848	1.073	1.137	1.000	1.184
1830	0.961	1.366	0.995	1.225	1.008	1.017	0.990	1.073	1.109	0.635
1840	1.107	0.957	0.934	1.087	0.937	1.129	0.616	0.912	0.841	0.759
1850	0.912	1.007	1.202	1.284	0.980	1.058	1.051	1.093	1.040	0.969
1860	0.745	0.892	0.992	0.812	1.111	0.913	0.895	0.831	1.112	0.971
1870	1.008	0.989	0.980	1.069	1.023	0.794	1.032	1.043	0.727	0.967
1880	0.958	1.187	0.979	1.016	1.269	1.142	0.831	0.813	0.899	0.725
1890	0.754	1.128	0.925	1.289	1.094	1.116	1.110	0.896	0.954	0.907
1900	0.965	0.908	1.078	0.837	1.251	1.216	0.919	0.734	0.782	0.837
1910	0.834	1.153	0.846	1.293	1.044	0.749	0.661	1.138	1.235	1.476
1920	1.114	1.109	1.005	0.909	1.057	0.965	0.813	0.972	0.668	0.843
1930	0.985	1.069	0.908	1.020	0.833	0.721	0.950	0.924	1.020	0.992
1940	1.415	0.954	1.111	0.899	1.082	0.859	0.750	0.917	0.772	1.097
1950	0.814	1.172	0.961	0.943	1.018	0.983	0.897	1.188	0.936	1.197
1960	0.822	1.227	0.945	1.568	1.082	1.100	0.995	1.085	0.834	0.828
1970	0.658	0.930	0.845	0.726	0.867	0.889	1.208	1.154	1.089	0.935
1980	0.978	1.114	1.376	1.102	1.124	1.228	1.307	1.023	0.915	1.043
1990	1.151	1.352	1.417	1.204	1.033	0.748	0.944	0.909	0.836	1.226
2000	1.237	1.234	1.366	–	–	–	–	–	–	

References

Ahmed M, Ogden J. 1985. Modern New Zealand tree-ring chronologies 3. *Agathis australis* (Salib.) – kauri. *Tree-Ring Bulletin* **45**: 11–24.

Ahmed M, Ogden J. 1987. Population dynamics of the emergent conifer *Agathis australis* (D. Don) Lindl. (kauri) in New Zealand: I. Population structures and tree growth rates in mature stands. *New Zealand Journal of Botany* **25**: 217–229.

Allan RJ. 1988. El Niño Southern Oscillation influences in the Australian region. *Progress in Physical Geography* **12**: 313–348.

Allan RJ. 2000. ENSO and climate variability in the past 150 years. In *El Niño and the Southern Oscillation: Multiscale Variability and Global and Regional Impacts*, Diaz HF, Markgraf V (eds). Cambridge University Press: Cambridge, 3–55.

Allan RJ, D'Arrigo RD. 1999. 'Persistent' ENSO sequences: how unusual was the 1990–1995 El Niño? *The Holocene* **9**: 101–118.

Allan RJ, Lindesay JA, Parker DE. 1996. *El Niño Southern Oscillation and Climatic Variability*. CSIRO Publications: Melbourne.

Basnett T, Parker D. 1997. *Development of the Global Mean Sea Level Pressure Data Set GMSLP2*. Climate Research Technical Note 79, Hadley Centre, United Kingdom Meteorological Office.

Berlage H. 1931. On the relationship between thickness of tree rings of Djati and rainfall on Java. *Tectona* **24**: 939–953.

Blasing TJ, Solomon AM, Duvick DN. 1984. Response functions revisited. *Tree-Ring Bulletin* **44**: 1–16.

Boswijk G, Ogden J. 2005. *Tree-ring Analysis of Kauri (Agathis Australis) from Hidden Valley, Great Barrier Island*. School of Geography and Environmental Science Working Paper 31, The University of Auckland, Auckland.

Boswijk G, Fowler A, Lorrey A, Palmer J, Ogden J. 2006. Extension of the New Zealand kauri (*Agathis Australis*) chronology to 1724 BC. *The Holocene* **16**: 188–199.

Briffa K, Jones P. 1990. Basic chronology statistics and assessment. In *Methods of Dendrochronology: Applications In The Environmental Sciences*, Cook E, Kairiukstis L (eds). Kluwer Academic: Dordrecht, 137–152.

Buckley B, Ogden J, Palmer J, Fowler AM, Salinger J. 2000. Dendroclimatic interpretation of tree-rings in *Agathis Australis* (kauri). 1. Climate correlation functions and master chronology. *Journal of the Royal Society of New Zealand* **30**: 263–275.

Cleaveland MK, Stahle DW, Therrell MD, Villanueva-Diaz J, Burns BT. 2003. Tree-ring reconstructed winter precipitation and tropical teleconnections in Durango, Mexico. *Climatic Change* **59**: 369–388.

Cook ER, Buckley BM, D'Arrigo RD, Peterson MJ. 2000. Warm-season temperatures since 1600 BC reconstructed from Tasmanian tree rings and their relationship to large-scale sea surface temperature anomalies. *Climate Dynamics* **16**: 79–91.

Cook ER, Palmer JG, Cook BI, Hogg A, D'Arrigo RD. 2002. A multi-millennial palaeoclimatic resource from *Lagarostrobos colensoi* tree-rings at Oroko Swamp, New Zealand. *Global and Planetary Change* **33**: 209–220.

D'Arrigo R, Jacoby G, Krusic P. 1994. Progress in Dendroclimatic Studies in Indonesia. *Terrestrial, Atmospheric and Oceanographic Sciences* **5**: 349–363.

D'Arrigo R, Cook ER, Wilson RJ, Allan R, Mann ME. 2005. On the variability of ENSO over the past six centuries. *Geophysical Research Letters* **32**(L03711): 1–4.

Diaz HF, Markgraf V (eds). 1992. *El Niño: historical and paleoclimatic aspects of the Southern Oscillation*. Cambridge University Press; Cambridge.

Diaz H, Markgraf V. 2000. *El Niño and the Southern Oscillation; Multiscale Variability and Global and Regional Impacts*. Cambridge University Press: New York.

DOI: 10.1002/joc

Diaz HF, Hoerling MP, Eischeid JK. 2001. ENSO variability, teleconnections and climate change. *International Journal of Climatology* **21**: 1845–1862.

Dunbar RB. 2000. El Niño – clues from corals. *Nature* **407**: 956–959.

Dunbar R, Wellington G, Colgan M, Glynn P. 1994. Eastern Pacific sea surface temperature since 1600 AD: the d18O record of climate variability in Galapagos corals. *Paleoceanography* **9**: 291–316.

Fowler A. 2005. Sea-level pressure composite mapping in dendroclimatology: advocacy and an *Agathis Australis* (kauri) case study. *Climate Research* **29**: 73–84.

Fowler A. 2007. ENSO history recorded in *Agathis australis* (kauri) tree rings. Part B: 423 years of ENSO robustness. *International Journal of Climatology* DOI: 10.1002/joc.1479.

Fowler A, Adams K. 2004. Twentieth century droughts and wet periods in Auckland (New Zealand) and their relationship to ENSO. *International Journal of Climatology* **24**: 1947–1961.

Fowler A, Boswijk G, Ogden J. 2004. Tree-ring studies on *Agathis australis* (kauri): a synthesis of development work on Late Holocene chronologies. *Tree-Ring Research* **59**: 53–62.

Fowler A, Lorrey A, Crossley P. 2005. Seasonal growth characteristics of kauri. *Tree-Ring Research* **61**: 3–20.

Fowler A, Palmer J, Salinger J, Ogden J. 2000. Dendroclimatic interpretation of tree-rings in *Agathis australis* (kauri): 2. Evidence of a significant relationship with ENSO. *Journal of the Royal Society of New Zealand* **30**: 277–292.

Fritts HC. 1976. *Tree Rings and Climate*. Academic Press: London.

Gergis J, Fowler A. 2005. Classification of synchronous oceanic and atmospheric El Niño-Southern Oscillation (ENSO) events for palaeoclimate reconstruction. *International Journal of Climatology* **25**: 1541–1565.

Gergis J, Fowler A, Mooney S. 2004. *A Multiproxy Analysis of El Nino Southern Oscillation (ENSO) Variability*. In 1st International CLIVAR Science Conference: Understanding and Predicting Our Climate System, June 21–25, 2004 Baltimore. Maryland.

Gergis J, Boswijk G, Fowler A. 2005a. *An Update of Modern Northland Kauri (Agathis Australis) Tree-Ring Chronologies 1: Puketi State Forest*. Working paper 29, School of Geography and Environmental Science, The University of Auckland, Auckland.

Gergis J, Boswijk G, Fowler A. 2005b. *An Update of Modern Northland Kauri (Agathis Australis) Tree-Ring Chronologies 2: Trounson Kauri Park*. Working paper 30, School of Geography and Environmental Science, The University of Auckland, Auckland.

Gordon ND. 1985. The Southern Oscillation: a New Zealand perspective. *Journal of the Royal Society of New Zealand* **15**: 137–155.

Gordon ND. 1986. The Southern Oscillation and New Zealand weather. *Monthly Weather Review* **114**: 371–387.

Hendy E, Gagan M, Lough J. 2003. Chronological control of coral records using luminescent lines and evidence for non-stationarity ENSO teleconnections in northeastern Australia. *The Holocene* **13**: 187–199.

Hendy EJ, Gagan MK, Alibert CA, McCulloch MT, Lough JM, Isdale PJ. 2002. Abrupt decrease in tropical Pacific sea surface salinity at end of Little Ice Age. *Science* **295**: 1511–1514.

Holmes RL, Adams RK, Fritts HC. 1986. Users manual for Program ARSTAN. In *Tree-Ring chronologies of Western North America: California, Eastern Oregon and Northern Great*. The University of Arizona: Tuscon, AZ. 50–60.

Jiang N, Hay JE, Fisher GW. 2004. Classification of New Zealand synoptic weather types and relation to the Southern Oscillation Index. *Weather and Climate* **23**: 3–24.

Kestin TS, Karoly DJ, Yano J-I. 1998. Time-frequency variability of ENSO and stochastic simulations. *Journal of Climate* **11**: 2258–2272.

Kidson JW. 2000. An analysis of New Zealand synoptic types and their use in defining weather regimes. *International Journal of Climatology* **20**: 299–316.

Konnen GP, Jones PD, Kaltofen MH, Allan RJ. 1998. Pre-1866 extensions of the Southern Oscillation Index using Early Indonesian and Tahitian Meteorological Readings. *Journal of Climate* **11**: 2325–2339.

Linsley B, Wellington G, Schrag D. 2000. Decadal Sea surface temperature variability in the subtropical South Pacific from 1726 to 1997 AD. *Science* **290**: 1145–1149.

Lorrey AM. 2005. Tree-ring analysis of kauri (*Agathis australis*) from Waitakere Reservoir, Waitakere Ranges, Auckland. Working Paper 23, School of Geography and Environmental Science, The University of Auckland, Auckland.

Lyons RG. 1997. *Understanding Digital Signal Processing*. Addison-Wesley Longman: Reading, Massachusetts.

Mann ME, Bradley RS, Hughes MK. 2000. Long-term variability in the El Niño/Southern Oscillation and associated teleconnections. In *El Niño and the Southern Oscillation: Multiscale Variability and Global and Regional Impacts*, Diaz HF and Markgraf V (ed). Cambridge University Press: Cambridge, 357–412.

Mullan AB. 1995. On the linearity and stability of Southern Oscillation-climate relationships for New Zealand. *International Journal of Climatology* **15**: 1365–1386.

Mullan AB. 1996. Non-linear effects of the Southern Oscillation in the New Zealand region. *Australian Meteorological Magazine* **45**: 83–99.

Ortlieb L. 2000. The documentary historical record of El Niño events in Peru: An update of the Quinn record (sixteenth through nineteenth centuries). In *El Niño and the Southern Oscillation: Multiscale Variability and Global and Regional Impacts*, Diaz HF and Markgraf V (ed). Cambridge University Press: Cambridge, 207–295.

Quenouille MA. 1952. *Associated Measurements*. Butterworths: London.

Quinn W, Neal V. 1992. The historical record of El Niño events. In *Climate Since A.D. 1500*, Bradley R and Jones P (ed). Routledge: London, 623–648.

Quinn TM, Crowley TJ, Taylor FW, Henin C, Joannot P, Join Y. 1998. A multicentury stable isotope record from a New Caledonia coral: interannual and Decadal Sea surface temperature variability in the Southwest Pacific since 1657 AD. *Paleoceanography* **13**: 412–426.

Reason CJC, Allan RJ, Lindesay JA, Ansell TJ. 2000. ENSO and climatic signals across the Indian Ocean Basin in the global context: part I, interannual composite patterns. *International Journal of Climatology* **20**: 1285–1327.

Salinger MJ, Mullan AB. 1999. New Zealand climate: temperature and precipitation variations and their links with atmospheric circulation 1930–1994. *International Journal of Climatology* **19**: 1049–1071.

Stahle DW, D'Arrigo RD, Krusic PJ, Cleaveland MK, Cook ER, Allan RJ, Cole JE, Dunbar RB, Therrell MD, Gay DA, Moore MD, Stokes MA, Burns BT, Villanueva-Diaz J, Thompson LG. 1998. Experimental Dendroclimatic Reconstruction of the Southern Oscillation. *Bulletin of the American Meteorological Society* **79**: 2137–2152.

Thompson LG, Mosley-Thompson E, Morales Arnao B. 1984. El nino-Southern Oscillation Events Recorded in the Stratigraphy of the Tropical Quelccaya Ice Cap, Peru. *Science* **226**: 50–53.

Thompson LG, Henderson KA, Mosley-Thompson E, Lin P-N. 2000. The tropical ice core record of ENSO. In *El Niño and the Southern Oscillation: Multiscale Variability and Global and Regional Impacts*, Diaz HF and Markgraf V (ed). Cambridge University Press: Cambridge, 325–356.

Torrence C, Compo GP. 1998. A practical guide to wavelet analysis. *Bulletin of the American Meteorological Society* **79**: 61–78.

Torrence C, Webster PJ. 1999. Interdecadal changes in the ENSO-monsoon system. *Journal of Climate* **12**: 2679–2690.

Trenberth KE, Caron JM. 2000. The Southern Oscillation revisited: sea level pressures, surface temperatures, and precipitation. *Journal of Climate* **13**: 4358–4365.

Trenberth KE, Stepaniak DP. 2001. Indices of El Niño evolution. *Journal of Climate* **14**: 1697–1701.

Van Oldenborgh GJ, Burgers G. 2005. Searching for decadal variations in ENSO precipitation teleconnections. *Geophysical Research Letters* **32**: L15304 10.1029/2005GL022847.

Wallace JM, Rasmusson EM, Mitchell TP, Kousky VE, Sarachik ES, von Storch H. 1998. On the structure and evolution of ENSO-related climate variability in the tropical Pacific: lessons from TOGA. *Journal of Geophysical Research* **103**: 14,241–14,259.

Whetton P, Rutherfurd I. 1994. Historical ENSO teleconnections in the Eastern Hemisphere. *Climatic Change* **28**: 221–253.

Wigley TML, Briffa KR, Jones PD. 1984. On the average value of correlated time series, with applications in dendroclimatology and hydrometeorology. *Journal of Climate and Applied Meteorology* **23**: 201–213.

Xiong L, Palmer JG. 2000. Reconstruction of New Zealand temperatures back to AD 1720 using *Libocedrus bidwillii* Tree-Rings. *Climatic Change* **45**: 339–359.